The diversity, structure and function of heritable adaptive immunity sequences in the *Aedes aegypti* genome

Zachary J. Whitfield[1*], Patrick T. Dolan[1,2*], Mark Kunitomi[1*#], Michel Tassetto[1], Matthew G. Seetin[3], Steve Oh[3], Cheryl Heiner[3], Ellen Paxinos[3], and Raul Andino[1]

[1] Department of Microbiology and Immunology, University of California, 600 16th Street, GH-S572, UCSF Box 2280, San Francisco, California 94143-2280, USA.

[2] Department of Biology, Stanford University, E200 Clark Center, 318 Campus Drive, Stanford, CA 94305

[3] Pacific Biosciences, 1305 O'Brien Drive, Menlo Park, California, 94025, USA.

*These authors contributed equally to this work

Current address: IBM Almaden Research Center, 650 Harry Road, San Jose, California, 95120-6099, USA.

To whom correspondence should be addressed. E-mail: raul.andino@ucsf.edu

Abstract

The *Aedes aegypti* mosquito is a major vector for arboviruses including dengue, chikungunya and Zika virus. Combating the spread of these viruses requires a more complete understanding of the mosquito immune system. Recent studies have implicated genomic endogenous viral elements (EVEs) derived from non-retroviral RNA viruses in insect immunity. Because these elements are inserted into repetitive regions of the mosquito genome, their large-scale structure and organization with respect to other genomic elements has been difficult to resolve with short-read sequencing. To better define the origin, diversity and biological role of EVEs, we employed single-molecule, real-time sequencing technology to generate a high quality, long-read assembly of the *Ae. aegypti*-derived Aag2 cell line genome. We leverage the quality and contiguity of this assembly to characterize the diversity and genomic context of EVEs in the genome of this important model system. We find that EVEs in the Aag2 genome are acquired through recombination by LTR retrotransposons, and organize into larger loci (>50kbp) characterized by high LTR density. These EVE containing loci are associated with increased transcription factor binding sight density and increased production of anti-genomic piRNAs. We also detected piRNA processing corresponding to on-going viral infection. This global view of EVEs and piRNA responses demonstrates the ubiquity and diversity of these heritable elements that define small-RNA mediated antiviral immunity in mosquitoes.

40

41 **INTRODUCTION (700 words currently)**

42 Arboviruses such as Dengue virus (DENV), Chikungunya virus (CHIKV),
43 and the newly emerging Zika virus, cause widespread and debilitating disease
44 across the globe (Bhatt et al., 2013). The primary vector of these viruses, *Aedes*
45 *aegypti,* has a global tropical/subtropical distribution (Kraemer et al., 2015)
46 creating distinct, geographically isolated populations. The genetic diversity of
47 *Aedes* populations has resulted in differential competence for vectoring virus
48 (Bennett et al., 2002). Differences in the insect immune system are critical factors
49 in determining competence (Kramer, 2016; Kramer & Ciota, 2015) and recent
50 studies suggest that virus-derived sequences in the mosquito genome may
51 contribute to resistance (Kunitomi et al., submitted). Comparative genomics may
52 explain these differences in vector competence between *Ae. aegypti* populations,
53 however the repetitive nature of the mosquito genome has been refractory to
54 assembly.

55 The genomic acquisition of viral sequences represents an important
56 source of genomic diversity and immune innovation in eukaryotes (Aswad &
57 Katzourakis, 2012; Chuong, Elde, & Feschotte, 2016; Feschotte & Gilbert, 2012;
58 Katzourakis & Gifford, 2010). Most virus-derived sequences are retroviral and are
59 acquired through the process of proviral genomic integration. Many examples of
60 acquired retroviral genes evolving new functions within the host have been
61 described (Chuong, et al., 2016). In addition, many sequences originating from
62 non-retroviruses have integrated into the genomes of their eukaryotic hosts.

63 These non-retroviral endogenous viral elements (EVEs) are thought to be
64 acquired through the action of endogenous retrotransposon-derived reverse
65 transcriptases (Belyi, Levine, & Skalka, 2010a, 2010b; Gilbert & Feschotte, 2010;
66 Horie et al., 2010; Katzourakis & Gifford, 2010; Taylor, Leach, & Bruenn, 2010).
67 Consistent with this model, DNA derived from RNA viruses is produced in
68 persistently infected *Drosophila* cell lines (Goic et al., 2013) and in infected
69 *Aedes albopictus* mosquitoes (and multiple mosquito-derived cell culture lines).
70 Synthesis of this viral DNA (vDNA) depends on the activity of endogenous
71 reverse transcriptases (Goic et al., 2016; Goic, et al., 2013). Furthermore,
72 sequencing of viral DNA isolated from *Drosophila* cell lines (Goic, et al., 2013)
73 has demonstrated the formation of recombinants between viral DNA sequences
74 and transposable elements.

75 Insects rely on RNAi-based immune defenses, wherein viral dsRNA
76 intermediates are recognized and processed through a dicer- and argonaute-
77 mediated pathway, ultimately leading to cleavage of viral RNA and protection
78 from infection (Mongelli & Saleh, 2016). Mosquitoes employ an additional RNAi
79 pathway which was previously associated primarily with TE silencing in
80 Drosophila, as an antiviral defense system (Hess et al., 2011; Miesen, Joosten, &
81 van Rij, 2016) (Kunitomi et al, submitted). The Piwi-interacting RNA (piRNA)
82 pathway, mediated by Piwi proteins and associated 24-28nt small RNAs,
83 involves the cleavage and processing of endogenous TE genomic antisense
84 transcripts into small RNAs. These small RNAs target TE transcripts with

85 appropriate sequence identity, yielding sense piRNAs that, in turn, drive further
86 antisense transcript processing.

87 Transcripts derived from genomic EVE sequences can be processed into
88 piRNAs, and a set of proteins responsible for their processing and maturation
89 has been identified (Arensburger, Hice, Wright, Craig, & Atkinson, 2011; Goic, et
90 al., 2016; Miesen, Girardi, & van Rij, 2015; Miesen, Ivens, Buck, & van Rij, 2016;
91 Miesen, Joosten, et al., 2016; Varjak et al., 2017). Genomic EVE sequences
92 confer resistance to viruses that encode identical sequences, in association with
93 an accumulation of EVE-specific piRNAs (Kunitomi et al, submitted) (Miesen,
94 Joosten, et al., 2016). Thus, the library of acquired viral sequences in the
95 mosquito genome not only represents a record of the natural history of infection
96 in this important vector species, but also a potential reservoir of immune memory.
97 Understanding the acquisition of circulating viruses into these heritable genomic
98 loci has major implications for mosquito immunity and disease transmission.
99 Toward that end, recent publications have examined Flavivirus EVEs in both
100 wild-caught mosquitoes and mosquito-derived cell lines (Suzuki et al., 2017) and
101 nonretroviral EVEs across currently available genomic assemblies (Palatini et al.,
102 2017). These studies have demonstrated that EVEs integrate in association with
103 LTR sequences and integrate into genomic loci known as piClusters. However,
104 because of difficulties resolving these genomic regions the full diversity of EVE
105 sequences and their relationship to piRNAs derived from these sequences have
106 not been yet described in a systematic way.

107 Here, we report the first such study, which examines the structure and
108 genomic context of the collection of non-retroviral EVEs present in the *Aedes*
109 *aegypti*-derived Aag2 cell line genome. Using an improved genomic assembly
110 from long-read sequencing as the basis of our analysis, we characterize the
111 structure and composition of EVE-containing loci across the entire genome.
112 Additionally, we compare these data to small RNA sequencing data from Aag2
113 cells to assess the transcription and processing of small RNAs originating from
114 these loci to understand the form and potential antiviral function of these
115 important loci.

116 **RESULTS**

117 **Sequencing and Assembly of the Aag2 Genome**

118 Current assemblies of the *Ae. aegypti* genome are based on two
119 sequencing strategies: one produced with the Illumina sequencing platform
120 (hereto referred to as 'UCB') (Vicoso & Bachtrog, 2015) and one based on
121 conventional Sanger sequencing (hereto referred to as 'LVP') (Nene et al., 2007).
122 In both instances, the Liverpool strain of *Ae. aegypti* was sequenced (Table 1). A
123 more recent study used Hi-C to further organize the Sanger-based *Ae. aegypti*
124 assembly into chromosome level scaffolds (Dudchenko et al., 2017). Due to the
125 highly repetitive nature of the *Ae. aegypti* genome and EVEs' tendency to cluster
126 with transposable elements within such repetitive regions, many EVEs are likely
127 to be missing from the current *Ae. aegypti* assemblies, which are based on
128 relatively short read lengths (Nene, et al., 2007; Vicoso & Bachtrog, 2015).
129 Assessing the comprehensive genome-wide diversity and genomic context of

130 EVE sequences therefore requires an improved genomic assembly. To this end,
131 we employed single-molecule, real-time sequence technology (Pacific
132 Biosystems) to generate a long read assembly of the genome of the cell line
133 Aag2.

134 We achieved approximately 76-fold coverage of the *Ae. aegypti*-based
135 Aag2 genome using the Single Molecule Real Time (SMRT) sequencing platform
136 (P6/C4 chemistry) to shotgun sequence 116 SMRT cells generating 92.7 GB of
137 sequencing data with an average read length of 15.5 kb. We used Falcon and
138 Quiver to generate a *de novo* 1.7 Gbp assembly with a contig N50 of ~1.4 Mbp.
139 Our draft assembly improves upon previous *Aedes* assemblies as measured by
140 N50, L50, and by contig number (Table 1 and Figure 1a). A majority of the Aag2
141 assembly sequence is found on contigs 10-100x longer than previous
142 assemblies. This increased contiguity allows the mapping of numerous contigs
143 from the initial LVP assembly to single Aag2 contigs (SI Figure 1), and makes for
144 an overall more ordered genome assembly.

145

146 **Repetitive nature of the Aag2 genome**

147 The genome of *Ae. aegypti* was previously shown to contain high
148 proportions of repeat-DNA (Nene, et al., 2007). The *Ae. aegypti*-derived Aag2
149 genome is no different, and is comprised of almost 55% repeat sequence (Table
150 1 and Table 2). Our sequencing strategy allows more repeats to be sequenced
151 within a single read, and therefore better reflects the structure and organization
152 of these repetitive elements. Direct alignment of contigs in the Aag2 assembly

153 and those of previous *Ae. aegypti* assemblies reveal resolved rearrangements
154 and distinct repeated regions that were collapsed into single sequences in the
155 previous assemblies (Figure 1b and SI Figure 1). These regions can span 10-
156 20kb (uncollapsed), illustrating the need for long read lengths to properly order
157 the vast number of repetitive regions in the *Ae. aegypti* genome. Of these
158 repetitive regions, over 75% are made up of transposon-derived sequence (Table
159 2).
160

161 **Identification of EVEs in the Aag2 genome**

162 Given their propensity to integrate into long, repetitive TE clusters (Figure
163 3c, 4b)(Parrish et al., 2015), our understanding of the EVE composition and
164 structure has been limited. Our improved, long-read assembly can better define
165 the complete set of EVEs contained within the Aag2 genome, hereby called the
166 "EVEome". Using a BLASTx-based approach, EVEs were identified with respect
167 to each virus' protein coding/(+)-sense strand (see Methods). We identified a
168 total of 472 EVEs in our Aag2 genome assembly. These EVEs represented at
169 least 8 annotated viral families, but were dominated by sequences derived from
170 Rhabdoviridae, Flaviviridae, and Chuviridae. The identified EVEs covered
171 338,251 bp and ranged from 50 to 2,520 bp length with a median length of 620
172 bp (Figure 2a and b).

173 To determine whether any region of the virus genome is more frequently
174 acquired, EVEs were mapped onto the viral ORFs from which they derive. This
175 analysis revealed asymmetric incorporation of certain viral ORFs (Figure 2c).

176 *Flaviviridae*-derived EVEs (Figure 2c, i) primarily mapped toward the 5' end of
177 the single Flaviviral ORF, leaving a relative dearth of EVEs at the 3' end. EVEs
178 deriving from *Rhabdoviridae* primarily originate from the Nucleoprotein (N) and
179 Glycoprotein (G) coding sequences, with only a few originating from the RNA-
180 dependent RNA polymerase (L) (Figure 2c, i). The lack of EVEs mapping to the
181 polymerase may be the result of RNA expression levels, with L being the least
182 expressed gene (Conzelmann, 1998), suggesting that the template for cDNA
183 synthesis is viral mRNA. The lack of EVEs originating from the Phosphoprotein
184 (P) or Matrix protein (M) is more difficult to explain, potentially reflecting the
185 availability of the RNA template for recombination, or deleterious effects
186 associated with acquisition of these sequences. Interestingly, EVEs derived from
187 Chuviridae primarily map to the ORF of the Glycoprotein. Given the diverse
188 Chuviridae genome organization (which occur as unsegmented, bi-segmented,
189 and possibly circularized negative-sense genomes)(Li et al., 2015), this pattern
190 could also be the result of mRNA abundance, or other mechanistic peculiarities
191 of Chuviridae interaction with EVE acquisition machinery (see below). Within
192 each viral ORF, there is no obvious preference for EVEs from a specific location.
193

194 **Comparison of EVEs in *Ae. aegypti* and *Aedes albopictus* genomes**

195 If EVEs serve as a representative record of viral infection over time, we
196 hypothesized that EVEs present in two different species of mosquito would also
197 differ (particularly given the relatively rare occurrence of genome fixation)
198 (Holmes, 2011; Katzourakis & Gifford, 2010). The *Ae. aegypti* and *Ae. albopictus*

199 species of mosquito occupy distinct (yet overlapping) regions around the globe
200 (Kraemer, et al., 2015) and have, therefore, faced different viral challenges over
201 time. While the EVEs present in the Aag2 and LVP *Ae. aegypti*-based genomes
202 correspond well, *Ae. aegypti* and *Ae. albopictus* do not share any specific EVEs.
203 However, exploring the Flaviviridae family of viruses in greater detail, the viral
204 species from which these EVEs are derived do primarily overlap (Figure 2d).
205 However, the relative abundance of EVEs derived from various viral species in
206 *Ae. aegypti* and *Ae. albopictus* differs. The lack of specific EVEs in common
207 between the mosquito genomes indicates EVE acquisition by *Ae. aegypti and*
208 *Ae. albopictus* occurred post-speciation, an important factor when considering
209 any differences in vector competence between these two species. However, it is
210 also important to note that these species are estimated to have diverged around
211 71 million years ago (Chen et al., 2015), and so only under very strong and
212 consistent positive selection could EVEs integrated pre-speciation have been
213 preserved.
214

215 **Insights into the mechanism of EVE integration**

216 Transposable elements (TEs) provide an important source of genomic
217 variation that drives evolution by modifying gene regulation and genome
218 organization, and through the acquisition of non-retroviral EVE sequences
219 (Gifford, Pfaff, & Macfarlan, 2013; Thompson, Macfarlan, & Lorincz, 2016).
220 Because of this relationship between transposable elements and EVE integration
221 (Feschotte & Gilbert, 2012; Honda & Tomonaga, 2016; Miesen, Joosten, et al.,

222 2016), and because our assembly is particularly suited for repeat identification
223 and analysis, we explored the organization of TEs, specifically focusing on those
224 proximal to EVE sequences.

225 The TEs in the Aag2 genome are derived from several different families
226 (Fig 3a, S1 Fig). Kimura distribution analysis of TEs in the Aag2 genome can be
227 used to 'date' the relative age of specific elements in the genome (Figure 3b)
228 (Kimura, 1980). The distributions of Kimura scores for TEs in our assembly
229 indicates relatively recent expansions of TEs, particularly LINE, LTR, and MITEs
230 elements (Figure 3b; low Kimura scores indicate TEs that are closer to the
231 element's consensus sequence, while higher scores indicated more diverged TE
232 sequences).

233 To determine whether a particular transposable element type is
234 responsible for EVE integration, we identified TEs whose position directly
235 overlaps EVE sequences (as called by RepeatMasker and BLASTX
236 respectively). This approach identifies mobile elements most likely responsible
237 for genomic integration of non-retroviral virus sequence. In line with observations
238 in *Ae. albopictus (Chen, et al., 2015)*, TEs overlapping EVE sequences are
239 greatly enriched for LTR retrotransposons (S2 Fig (i); p-value < $3x10^{-60}$). A
240 similar pattern was observed when classifying the nearest upstream and
241 downstream, non-overlapping TE sequences around each EVE (Figure 3c(i)).
242 These results further implicate LTR retrotransposons in the acquisition of EVEs
243 and indicate that the typical integration sites are composed of clusters of similar
244 LTR retrotransposons.

245 Strikingly, 543 out of 614 LTRs shared the same polarity as their nearest-
246 neighbor EVE (i.e. both TE and EVE elements are located on the same genomic
247 DNA strand). These 543 LTRs made up the vast majority of all TEs with the
248 same polarity as their nearest EVE (543/746; Figure 3c(i); p-value = 1.09×10^{-252}
249 by one-sided binomial test). This bias is consistent with a copy-choice
250 mechanism of recombination between LTR retrotransposon sequence and viral
251 RNA (or viral mRNA) leading to EVE integration, as previously proposed (Cotton,
252 Steinbiss, Yokoi, Tsai, & Kikuchi, 2016; Geuking et al., 2009). Our analysis of
253 transposons in the Aag2 genome shows LTR-retrotransposons display less
254 sequence diversity (by Kimura Divergence score; Figure 3b), indicating that they
255 are currently (or were recently) actively replicating in the Aag2 cell line.
256 Consistent with this idea, LTR-retrotransposon transcripts and proteins are
257 readily detected in Aag2 cells (Maringer et al., 2017). These data are consistent
258 with LTR-retrotransposons being responsible for the acquisition of the majority of
259 EVEs observed in the *Ae. aegypti*-derived Aag2 genome.

260 Within the LTR retrotransposon family, both Ty3/gypsy and Pao Bel TEs
261 are enriched surrounding EVEs (Figure 3c iv,v). Again, this enrichment for
262 Ty3/gypsy and Pao Bel elements near EVE loci is strongest when the EVE and
263 TE are in the same orientation (p-value = 6.90×10^{-29} and 1.71×10^{-3}
264 respectively). The drastic bias in associated transposons based on directionality
265 is not observed for other TE categories (Figure 3c, iii, vi). These data support
266 Ty3/gypsy (and to a lesser extent Pao Bel) as the primary transposon type
267 facilitating EVE genomic integration in the Aag2 cell line. Interestingly, an

268 association between LTR Ty3/gypsy elements and integrated viral sequence has
269 also been observed previously in plants (Lee, Nolan, Watson, & Tristem, 2013;
270 Staginnus et al., 2007), suggesting a conserved mechanism for the acquisition of
271 invading virus sequences and generation of EVEs.

272 EVE-proximal TEs of the Ty3/gypsy and Pao Bel families can be further
273 partitioned into individual elements. Of these, many specific elements were
274 enriched for being the nearest TE to an EVE (Figure 3c(iv, v)). Interestingly,
275 EVEs derived from different virus families show different patterns of enrichment
276 for nearby TEs (Figure 3d). Although Flaviviridae- and Rhabdoviridae-derived
277 EVEs show strong enrichment for Ty3/gypsy transposable elements, Chuviridae-
278 derived EVEs are associated with Pao Bel elements.

279

280 **EVEs associate with piClusters.**

281 The strong enrichment for multiple LTRs around EVEs (Fig 3c, S2 Fig) led
282 us to examine the genomic context of EVE-TE integration sites in the genome.
283 The large contig sizes associated with our long-read sequencing approach allow
284 us to assess the large-scale spatial distribution of TEs and EVEs in the genome.
285 Strikingly, we identified numerous loci where many EVE sequences overlapped
286 with large regions of increased LTR density, some larger than 50kbp in length
287 (Figure 4a). In some cases, these large loci are so densely packed with a single
288 LTR they effectively “crowd out” any other repetitive elements (Figure 4b). Within
289 these loci, EVE sequences are interspersed with TE fragments in unidirectional
290 orientations (Figure 4c). They contain large numbers of EVEs derived from

291 different viral families (Figure 4c-e) suggesting that these regions occasionally
292 capture new TE-virus hybrids.

293 The organization of these loci is similar to that of piClusters (Yamanaka,
294 Siomi, & Siomi, 2014): piRNA-producing loci in the genome that result from the
295 accumulation of TE fragments (due to non-random LTR integrase-directed
296 integration)(Lesbats, Engelman, & Cherepanov, 2016). To assess the ability of
297 these loci to produce piRNAs, we performed small RNA sequencing, employing a
298 procedure to enrich for *bona fide* piRNAs. Indeed, we found that these loci
299 produce a large number of piRNAs in a predominantly anti-sense orientation,
300 consistent with the transcription of piClusters (Czech & Hannon, 2016;
301 Yamanaka, et al., 2014).

302 We then used bioinformatic prediction to identify putative piClusters in the
303 genome based upon piRNA mapping density. This analysis identified 469 piRNA-
304 encoding loci (piClusters) using proTRAC (Rosenkranz, Rudloff, Bastuck,
305 Ketting, & Zischler, 2015; Rosenkranz & Zischler, 2012), accounting for
306 5,774,304 bp (0.335%) of the genome. Depending on the mapping algorithm
307 used, between 63% (bowtie) and 77% (sRNAmapper.pl, see Methods) of beta-
308 eliminated small RNAs from Aag2 cells mapped to these loci. Of the identified
309 piClusters, 65 (14.1%) have EVE sequences associated with them and 64 of
310 these piCluster-resident EVE sequences act as the template for piRNAs. Of the
311 472 EVEs identified, 256 (66.7%) or 280,475 bp of the 411,239 EVE bp mapped
312 to piClusters (68.2%, Fisher's test $p<2.2e-16$, OR=203.42). Furthermore, a vast
313 majority of piRNAs which map to EVEs are anti-sense to the coding sequence of

314 the corresponding virus (544,429/547,014; 99.5%), meaning that majority of
315 piRNAs produced from genomic EVEs are potentially antiviral.

316 To examine whether piCluster-resident EVEs are under selection we
317 examined the relative transcription of piClusters throughout the genome.
318 piClusters that contain EVEs tend to produce more piRNAs (Fig 4d,e) The
319 increased piRNA production at EVE-containing loci, is consistent with the
320 observation that piClusters with EVEs exhibit higher transcription factor binding
321 site density (Fig 4f). GATA4, SOX9 and RFX transcription factor binding sites are
322 all enriched near EVE-containing piClusters ($p<2E-16$, Wilcox rank-sum test).
323 These data together suggest that selection acts at the level of EVE-specific
324 piRNA production.

325

326 **piRNA abundance reflects the cellular immune state**

327 EVEs, in combination with their associate piRNAs, make up a reservoir of
328 small RNA immune memory. Notably, in the Aag2 cell line, piRNA production
329 from EVEs derived from a given viral family does not completely correlate with
330 genomic abundance of those EVEs, suggesting that the antiviral potential of the
331 EVEome against a given viral family depends on the amount of viral genetic
332 information stored in the host genome, the transcriptional activity of individual
333 piClusters and the sequence identity of the resulting piRNAs to circulating viral
334 challenges (Figure 5a,b).

335 To examine the potential antiviral activity of piRNAs that originate from
336 genomic EVEs, we mapped the same piRNA libraries (allowing for up to 3

337 mismatches) to contemporary viral genomes from which EVEs were expected to
338 have derived (Figure 5d, S5 Fig). Aag2 cells are known to be persistently
339 infected with cell-fusing agent virus (CFAV; *flaviviridae*), and were recently
340 shown to also be persistently infected with Phasi Charoen-like virus (PCLV;
341 *bunyaviridae*) (Maringer, et al., 2017) and these viruses, therefore, constitute
342 potential substrates for recognition by EVE-derived piRNAs and subsequent
343 processing. EVE-derived anti-genomic piRNAs (Figure 5c) only mapped to a
344 single site on the PCLV nucleocapsid. However, we identified numerous sense
345 piRNAs derived from PCLV, including a prominent peak which is offset from the
346 EVE-derived anti-sense piRNA binding site by 10bps (Figure 5d,e). This pattern
347 is consistent with EVE-derived piRNAs being funneled through canonical
348 processing by the ping-pong amplification mechanism, being successfully loaded
349 into the Piwi machinery and subsequently cleaving the viral mRNA. A similar
350 pattern was observed for CFAV (Kunitomi, et al, submitted). Mapping of piRNAs
351 to other viruses from which EVEs derived do not reveal this 'response' sense
352 piRNA peak, presumably because those viruses are not currently replicating in
353 the cells (S5 Fig). These observations indicate that an organism's EVEome
354 produces piRNAs capable of recognizing viruses and initiating an active
355 response.
356

357 **DISCUSSION**

358

359 A solid foundation with which to study the genetic factors contributing to
360 vector competence is of utmost importance as arboviruses become an increasing
361 burden globally. *In vivo* studies of mosquito immunity are a valuable but
362 challenging approach to understanding arboviral life cycles. With this in mind, we
363 generated a long-read assembly of the *Aedes aegypti* cell line, Aag2. With this
364 highly contiguous assembly, we then identified nearly the entire set of
365 endogenous viral elements and their surrounding genomic context in the Aag2
366 cell line at a genome-wide scale. The Aag2 cell line is an important model system
367 for the characterization of arboviral replication in mosquito hosts. Considering the
368 potential impact of EVE sequences and their associated piRNAs on viral
369 infection, understanding the diversity of EVEs in commonly used cell lines is
370 especially important.

371 Surveying the genome-wide collection of EVEs in the Aag2 genome
372 provides not only a view of the historical interactions between host and virus, but
373 also the repertoire of acquired sequences that define the piRNA-based immune
374 system of this important model system. Our analysis refines our understanding of
375 EVEs in the *Ae. aegypti* genome, their relationship to transposable elements, and
376 the potential breadth of antiviral protection they provide. We propose that a
377 mosquito's EVEome, together with the piRNA system, represents a potentially
378 long-lasting branch of its RNAi anti-viral defense system. Although all mosquito
379 species share the same basic RNAi-based immune system, the differences in the

380 EVEome of a given species, subpopulation, or individual, such as those
381 observed between *Ae. aegypti* and *Ae. albopictus* (Figure 2a), may represent a
382 factor contributing to inherent differences in vector competence across many
383 different scales. Indeed, the EVEome of wild mosquito populations appears to be
384 in rapid flux (Varjak, et al., 2017).

385 The presence of piRNA producing EVEs in the *Ae. aegypti* genome is
386 reminiscent of the CRISPR system in bacteria. Both take advantage of the
387 invading pathogen's genetic material to create small RNAs capable of restricting
388 an invading virus' replication. Furthermore, both integrate into the host's
389 genome, potentially providing protection against infection across generations.
390 Although the conservation of this pathway across Eukarya is not yet clear, recent
391 publications have highlighted the integration of genetic material from non-
392 retroviral RNA viruses into the genome of many different host species during
393 infection. The antiviral activity of these sequences has not been established,
394 however, a subset of EVEs found in mammalian systems seem to be under
395 purifying selection, suggesting some potential benefit to the host (Horie, et al.,
396 2010). In contrast to the evolutionary repurposing of retroviral sequences, the
397 direct integration, transcription and processing of EVE sequences into antiviral
398 small RNAs constitutes a mechanism by which these acquired sequences can be
399 rapidly repurposed for host immune purposes.

400 Template switching during reverse transcription has previously been
401 proposed to play a role in creating transposon-virus hybrids which integrate into
402 the host genome to form EVEs (Cotton, et al., 2016; Geuking, et al., 2009). The

403 apparent family-level specificity observed between Pao Bel TEs and Chuviridae-
404 derived sequences and between Ty3/gypsy TEs and Flaviviridae and
405 Rhabdoviridae sequences is interesting in this respect (Figure 3d). This could
406 have occurred by chance, or may hint at an even deeper level of specificity
407 directing capture of viral sequences by LTRs. Possibly these TEs and viruses
408 share increased sequence homology leading to more frequent template switching
409 (Delviks-Frankenberry et al., 2011), or replicate in a similar subcellular location. It
410 is also possible that LTR/EVE pairs were selected for and maintained after EVE
411 integration into the mosquito genome. Suzuki et al. note that in different strains of
412 *Ae. albopictus*, the Flavivirus-derived EVEs are conserved, but their flanking
413 regions can be quite distinct (Suzuki, et al., 2017). As the authors noted, this
414 hints at an evolutionary role for the EVEs themselves, but not necessarily the
415 specific surrounding regions. Given the difference in piRNA production among
416 piClusters with EVEs and without (Figure 4d,e), selection may only act at the
417 level of piRNA production, rather than the specific TE elements.

418 Uncovering the genomic context of EVEs highlights the potential for the
419 piRNA system to shape the mosquito immune system. It also provides a
420 foundation for future investigations into EVE function. Comparative genomic
421 approaches that incorporate long-read sequencing to understand the diversity of
422 the EVEome across populations will allow us to better understand the forces that
423 underlie the epidemiology and population dynamics of arboviruses. Moreover,
424 the potential to manipulate this heritable, anti-viral immune system could present

425 opportunities for epidemiological interventions in natural settings, or as a genetic
426 system to understand the insect immune system in the laboratory.
427
428
429 **Acknowledgements**
430 We thank Dr. Kevin M. Dalton for helpful discussion and code for the analysis.
431

432 **MATERIALS AND METHODS**
433 **Cells culture**
434 *Aedes aegypti* Aag2 *(Lan & Fallon, 1990; Peleg, 1968)* cells were cultured
435 at 28 °C without CO_2 in Schneider's *Drosophila* medium (GIBCO-Invitrogen),
436 supplemented with 10% heat-inactivated fetal bovine serum (FBS), 1X non-
437 essential amino acids (NEAA, UCSF Cell Culture Facility, 100X stock is 0.1 µM
438 filtered, 10 mM each of Glycine, L-Alanine, L-Asparagine, L-Aspartic acid, L-
439 Glutamic Acid, L-Proline, and L-Serine in de-ionized water), and 1X Penicillin-
440 Streptomycin-Glutamine (Pen/Strep/G, 100X = 10,000 units of penicillin, 10,000
441 µg of streptomycin, and 29.2 mg/ml of L-glutamine, Gibco).
442
443 **DNA sequencing**
444 Aag2 cells were grown in T-150 Flasks until ~80% confluent. Cells were
445 then washed with dPBS twice and scrapped off in dPBS + 10 µg/ml RNase A
446 (ThermoFisher). Genomic DNA (gDNA) was extracted from ~10^8 Aag2 cells
447 using the QIAamp DNA Mini Kit according to the manufacturer's instructions with
448 the optional RNase A treatment. Aag2 gDNA was re-suspended in 10mM Tris
449 pH8, and the quality and quantity of the sample was assessed using the Agilent
450 DNA12000 kit and 2100 Bioanalyzer system (Agilent Technologies), as well as
451 the Qubit dsDNA Broad Range assay kit and Qubit Fluorometer (Thermo Fisher)
452 and visualized by gel electrophoresis (1% TBE gel). After purification and
453 quality control, a total of 130 ug of DNA was available for library preparation and
454 sequencing.
455 SMRTbell libraries were prepared using Pacific Biosciences' Template
456 Prep Kit 1.0 (PacBio) and a slightly modified version of the Pacific Biosciences'
457 protocol, "Procedure & Checklist - 20-kb Template Preparation Using BluePippin
458 Size-Selection System (15-kb Size Cutoff)". Specifically, 52.5ug of gDNA were
459 hydrodynamically sheared to target sizes of 30kb (26 µg) and 35 kb (26 µg) using
460 the Megaruptor® (Diogenode) with long hydropores according to the
461 manufacturer's protocols. Size distributions of the final sheared gDNA were
462 verified by pulse field electrophoresis of a 100ng sub-aliquot through 0.75%
463 agarose using the Pippin Pulse (Sage Science), run according to the
464 manufacturer's "10-48 kb protocol" for 16 hrs. The two sheared samples were
465 then pooled, for a total of 37ug sheared DNA to be used as input into SMRTbell
466 preparation. Sheared DNA was subjected to DNA damage repair and ligated to
467 SMRTbell adapters. Following ligation, extraneous DNA was digested with exo-
468 nucleases and the resulting SMRTbell library was cleaned and concentrated with
469 AMPure PB beads (Pacific Biosciences). A total of 20.5ug of library was available
470 for size selection.
471 Approximately half (10ug) of the SMRTbell pooled SMRTbell library was
472 size-selected using the BluePippin System (Sage Science) using a 15 kb cutoff
473 and 0.75% agarose cassettes. To obtain longer read lengths, an additional 5ug
474 of the library was selected using a 17kb cutoff.
475 Library quality and quantity were assessed using the Agilent 12000 DNA
476 Kit and 2100 Bioanalyzer System (Agilent Technologies), as well as the Qubit
477 dsDNA Broad Range Assay kit and Qubit Fluorometer (Thermo Fisher). An

additional DNA Damage Repair step and AMPure bead cleanup were included after size-selection of the libraries.

Annealed libraries were then bound to DNA polymerases using 3nM of the SMRTbell library and 3X excess DNA polymerase at a concentration of 9nM using Pacific Biosciences DNA/Polymerase Binding Kit 1.0, (Pacific Biosciences). Bound libraries were sequenced on the Pacific Biosciences RSII using P6/C4 chemistry (PacBio), magnetic bead loading (PacBio) and 6 hour collection times. 84 SMRTcells of the > 15 kb library were loaded at concentrations of 75-100 pM on-plate. 32 SMRTcells of the > 17 kb library was prepared separately and loaded at on-plate concentrations of 40 pM and 60 pM. These 116 SMRTcells generated 92.7 GB of sequencing data, which resulted in approximately 76X coverage of the Aag2 genome. Average raw read length of 15.5KB, with average sub-reads length of 13.2kb. Assembly was performed using Quiver/FALCON

Genome assembly statistics

Basic statistics (e.g. Size, Gaps, N50, L50, # contigs) for each genome analyzed was produced using Quast (Gurevich, Saveliev, Vyahhi, & Tesler, 2013).

As a complementary approach Benchmarking sets of Universal Single-Copy Orthologs (BUSCO) was also run using the Arthropod dataset in order to assess the completeness of genome assembly. Of the 2675 BUSCO groups searched only 81 were missing from the Aag2 assembly, indicating good assembly completeness. Of the 2315 BUSCOs found only 279 of them were annotated as fragmented, emphasizing the continuity of the assembly.

Repeat Identification and Kimura Divergence

In order to *de novo* identify and classify novel repetitive elements from the Aag2 genome, RepeatModeler was run on the assembled genome using standard parameters. Outputs from RepeatModeler were cross-referenced with annotated entries for Aedes aegypti from TEfam. All entries from RepeatModeler that were >80% identical to TEfam entries were discarded as redundant. This combined annotated and de novo identified list of repeat elements was used to identify the genome wide occurrences of repeats using RepeatMasker using standard parameters.

Kimura scores and corresponding alignment information were extracted from the ".align" file as output by RepeatMasker. This information was used to make the stacked plot in figure 2 using R (version 3.30) and the ggplot2 package.

Citations:

Smit, AFA, Hubley, R. *RepeatModeler Open-1.0*. 2008-2015 <http://www.repeatmasker.org>

Smit, AFA, Hubley, R & Green, P. *RepeatMasker Open-4.0*. 2013-2015 <http://www.repeatmasker.org>.

Dr. Zhijian Jake Tu. TEfam. <http://tefam.biochem.vt.edu/tefam/index.php>

524 **EVE identification**

525 Identification of EVEs was achieved using standalone Blast+ (Altschul,
526 Gish, Miller, Myers, & Lipman, 1990). Blast Searches were run using the Blastx
527 command specifying the genome as the query and a refseq library composed of
528 the ssRNA and dsRNA viral protein-coding sequences from the NCBI genomes
529 as the database. The E-value threshold was set at 10-6.

530 The EVE with the lower E-value was chosen for further analysis to predict
531 EVEs that overlapped. Several Blast hits to viral protein genes were identified as
532 artifacts because of their homology to eukaryotic genes (e.g. closteroviruses
533 encode an Hsp70 homologue). These artifacts were filtered by hand.

534

535 **Identification of LTR enrichment near EVEs**

536 Separate BED files containing all TEs in the Aag2 assembly and all EVEs
537 in the Aag2 assembly were used as input to Bedtools (*bedtools closest* command
538 using the *–io* flag, and *–id* or *-iu*) to find the single closest non-overlapping TE to
539 each EVE (both upstream and downstream).

540 An in-house script compiled these two output files together and filtered
541 them for the TE content of interest. TE categories (subclass, family, element)
542 were assigned by RepeatMasker. Enrichment was compared to the prevalence
543 of the TE element genome wide based on a one-sided binomial test. Stacked
544 histograms were produced based on TE categories as found in Figure 3. The
545 legend lists (up to) the 10 most prevalent TE elements of TE/EVE pairs in the
546 same orientation. Plots were produced using Python (version 2.7.6) with the
547 pandas and matplotlib plugins.

548

549 **Classification of nearest TE to EVEs by virus taxonomy**

550 Taxonomy categories for viruses from which each EVEs derived were
551 assigned using an in-house script. Assignments were made based on NCBI's
552 taxonomy database (ftp://ftp.ncbi.nih.gov/pub/taxonomy/), with the following
553 additional annotations by hand.

554

Virus species	Assigned family
Wuhan Mosquito Virus 8	Chuviridae
Wuchang Cockraoch Virus 3	Chuviridae
Lishi Spider Virus 1	Chuviridae
Shayang Fly Virus 1	Chuviridae
Wenzhou Crab Virus 2	Chuviridae
Bole Tick Virus 2	Rhabdoviridae
Shayang Fly Virus 2	Rhabdoviridae
Wuhan Ant Virus	Rhabdoviridae
Wuhan Fly Virus 2	Rhabdoviridae
Wuhan House Fly Virus 1	Rhabdoviridae
Wuhan Mosquito Virus 9	Rhabdoviridae

Yongjia Tick Virus 2	Rhabdoviridae
Cilv-C	Virgaviridae
Citrus leprosis virus C	Virgaviridae
Blueberry necrotic ring blotch virus	Virgaviridae
Wutai Mosquito Virus	Bunyaviridae

Heat maps were produced using the Seaborn plugin for python. Only TEs with >=10% proportion in at least one sample (Flaviviridae, Chuviridae, or Rhabdoviridae) are shown. Color was assigned based on proportion of TE element/family in each viral category.

Enrichment was scored as above using a one-sided binomial test (significant is p-value < 0.0001).

Small RNA bioinformatics

Adaptors were trimmed using Cutadapt (http://dx.doi.org/10.14806/ej.17.1.200) using the --discard-untrimmed and -m 19 flags to discard reads without adaptors and below 19 nt in length. Reads were mapped using bowtie (Langmead, Trapnell, Pop, & Salzberg, 2009)using the –v 1 flag (- v 3 in the case of Fig 5D and S5). Read distance overlaps were generated by viROME (Watson, Schnettler, & Kohl, 2013). Uniquely mapping piRNAs were used for Figure 4C (- m1 flag).

piCluster Analysis

piClusters were identified using PROtrac (Rosenkranz & Zischler, 2012) based on mapping with positions for beta-eliminated small RNAs libraries from Aag2 cells from sRNAmapper.pl. Based on these predictions, visualizations of clusters were produced using EasyFig (Sullivan, Petty, & Beatson, 2011) for visualization of TEs and R for comparison of TEs, piRNA abundance and EVE positions.

Sequence alignment and phylogenetic analysis

For phylogenetic analysis of Flaviviridae, polyprotein sequences from 61 members of the Flaviviridae family were aligned with MUSCLE (Edgar, 2004) and a maximum likelihood tree was generated with FastTree (Price, Dehal, & Arkin, 2009) using the generalised time reversible substitution model ("-gtr"). Trees were visualized and annotated with ggtree (DOI: 10.1111/2041-210X.12628).

EVE coverage

Base R (version 3.3.0) was used to show regions individual EVEs span on the indicated viral family (and protein). EVE length is a function of the percentage of the respective ORF from which it derives.

Data availability

The Aag2 genome (v 1.00) is available through VectorBase (https://www.vectorbase.org/organisms/aedes-aegypti/aag2/aag2).
Main datasets produced during this work have been provided in excel format.

REFERENCES

Altschul, S. F., Gish, W., Miller, W., Myers, E. W., & Lipman, D. J. (1990). Basic local alignment search tool. *J Mol Biol, 215*(3), 403-410. doi: 10.1016/S0022-2836(05)80360-2
S0022-2836(05)80360-2 [pii]

Arensburger, P., Hice, R. H., Wright, J. A., Craig, N. L., & Atkinson, P. W. (2011). The mosquito Aedes aegypti has a large genome size and high transposable element load but contains a low proportion of transposon-specific piRNAs. *BMC Genomics, 12*, 606. doi: 10.1186/1471-2164-12-606
1471-2164-12-606 [pii]

Aswad, A., & Katzourakis, A. (2012). Paleovirology and virally derived immunity. *Trends Ecol Evol, 27*(11), 627-636. doi: 10.1016/j.tree.2012.07.007
S0169-5347(12)00168-1 [pii]

Belyi, V. A., Levine, A. J., & Skalka, A. M. (2010a). Sequences from ancestral single-stranded DNA viruses in vertebrate genomes: the parvoviridae and circoviridae are more than 40 to 50 million years old. *J Virol, 84*(23), 12458-12462. doi: 10.1128/JVI.01789-10
JVI.01789-10 [pii]

Belyi, V. A., Levine, A. J., & Skalka, A. M. (2010b). Unexpected inheritance: multiple integrations of ancient bornavirus and ebolavirus/marburgvirus sequences in vertebrate genomes. *PLoS Pathog, 6*(7), e1001030. doi: 10.1371/journal.ppat.1001030

Bennett, K. E., Olson, K. E., Munoz Mde, L., Fernandez-Salas, I., Farfan-Ale, J. A., Higgs, S., . . . Beaty, B. J. (2002). Variation in vector competence for dengue 2 virus among 24 collections of Aedes aegypti from Mexico and the United States. *Am J Trop Med Hyg, 67*(1), 85-92.

Bhatt, S., Gething, P. W., Brady, O. J., Messina, J. P., Farlow, A. W., Moyes, C. L., . . . Hay, S. I. (2013). The global distribution and burden of dengue. *Nature, 496*(7446), 504-507. doi: 10.1038/nature12060
nature12060 [pii]

Chen, X. G., Jiang, X., Gu, J., Xu, M., Wu, Y., Deng, Y., . . . James, A. A. (2015). Genome sequence of the Asian Tiger mosquito, Aedes albopictus, reveals insights into its biology, genetics, and evolution. *Proc Natl Acad Sci U S A, 112*(44), E5907-5915. doi: 10.1073/pnas.1516410112
1516410112 [pii]

Chuong, E. B., Elde, N. C., & Feschotte, C. (2016). Regulatory evolution of innate immunity through co-option of endogenous retroviruses. *Science, 351*(6277), 1083-1087. doi: 10.1126/science.aad5497
351/6277/1083 [pii]

Conzelmann, K. K. (1998). Nonsegmented negative-strand RNA viruses: genetics and manipulation of viral genomes. *Annu Rev Genet, 32*, 123-162. doi: 10.1146/annurev.genet.32.1.123

Cotton, J. A., Steinbiss, S., Yokoi, T., Tsai, I. J., & Kikuchi, T. (2016). An expressed, endogenous Nodavirus-like element captured by a retrotransposon in the genome of the plant parasitic nematode Bursaphelenchus xylophilus. *Sci Rep, 6*, 39749. doi: 10.1038/srep39749
srep39749 [pii]

Czech, B., & Hannon, G. J. (2016). One Loop to Rule Them All: The Ping-Pong Cycle and piRNA-Guided Silencing. *Trends Biochem Sci, 41*(4), 324-337. doi: 10.1016/j.tibs.2015.12.008

646 S0968-0004(15)00258-3 [pii]
647 Delviks-Frankenberry, K., Galli, A., Nikolaitchik, O., Mens, H., Pathak, V. K., & Hu, W. S.
648 (2011). Mechanisms and factors that influence high frequency retroviral
649 recombination. *Viruses, 3*(9), 1650-1680. doi: 10.3390/v3091650
650 viruses-03-01650 [pii]
651 Dudchenko, O., Batra, S. S., Omer, A. D., Nyquist, S. K., Hoeger, M., Durand, N. C., . . .
652 Aiden, E. L. (2017). De novo assembly of the Aedes aegypti genome using Hi-C
653 yields chromosome-length scaffolds. *Science*. doi: eaal3327 [pii]
654 10.1126/science.aal3327
655 science.aal3327 [pii]
656 Edgar, R. C. (2004). MUSCLE: multiple sequence alignment with high accuracy and high
657 throughput. *Nucleic Acids Res, 32*(5), 1792-1797. doi: 10.1093/nar/gkh340
658 32/5/1792 [pii]
659 Feschotte, C., & Gilbert, C. (2012). Endogenous viruses: insights into viral evolution and
660 impact on host biology. *Nat Rev Genet, 13*(4), 283-296. doi: 10.1038/nrg3199
661 nrg3199 [pii]
662 Geuking, M. B., Weber, J., Dewannieux, M., Gorelik, E., Heidmann, T., Hengartner, H., .
663 . . Hangartner, L. (2009). Recombination of retrotransposon and exogenous RNA
664 virus results in nonretroviral cDNA integration. *Science, 323*(5912), 393-396. doi:
665 10.1126/science.1167375
666 323/5912/393 [pii]
667 Gifford, W. D., Pfaff, S. L., & Macfarlan, T. S. (2013). Transposable elements as genetic
668 regulatory substrates in early development. *Trends Cell Biol, 23*(5), 218-226. doi:
669 10.1016/j.tcb.2013.01.001
670 S0962-8924(13)00003-2 [pii]
671 Gilbert, C., & Feschotte, C. (2010). Genomic fossils calibrate the long-term evolution of
672 hepadnaviruses. *PLoS Biol, 8*(9). doi: 10.1371/journal.pbio.1000495
673 e1000495 [pii]
674 Goic, B., Stapleford, K. A., Frangeul, L., Doucet, A. J., Gausson, V., Blanc, H., . . .
675 Saleh, M. C. (2016). Virus-derived DNA drives mosquito vector tolerance to
676 arboviral infection. *Nat Commun, 7*, 12410. doi: 10.1038/ncomms12410
677 ncomms12410 [pii]
678 Goic, B., Vodovar, N., Mondotte, J. A., Monot, C., Frangeul, L., Blanc, H., . . . Saleh, M.
679 C. (2013). RNA-mediated interference and reverse transcription control the
680 persistence of RNA viruses in the insect model Drosophila. *Nat Immunol, 14*(4),
681 396-403. doi: 10.1038/ni.2542
682 ni.2542 [pii]
683 Gurevich, A., Saveliev, V., Vyahhi, N., & Tesler, G. (2013). QUAST: quality assessment
684 tool for genome assemblies. *Bioinformatics, 29*(8), 1072-1075. doi:
685 10.1093/bioinformatics/btt086
686 btt086 [pii]
687 Hess, A. M., Prasad, A. N., Ptitsyn, A., Ebel, G. D., Olson, K. E., Barbacioru, C., . . .
688 Campbell, C. L. (2011). Small RNA profiling of Dengue virus-mosquito
689 interactions implicates the PIWI RNA pathway in anti-viral defense. *BMC*
690 *Microbiol, 11*, 45. doi: 10.1186/1471-2180-11-45
691 1471-2180-11-45 [pii]
692 Holmes, E. C. (2011). The evolution of endogenous viral elements. *Cell Host Microbe,*
693 *10*(4), 368-377. doi: 10.1016/j.chom.2011.09.002
694 S1931-3128(11)00285-X [pii]

695 Honda, T., & Tomonaga, K. (2016). Endogenous non-retroviral RNA virus elements
696 evidence a novel type of antiviral immunity. *Mob Genet Elements, 6*(3),
697 e1165785. doi: 10.1080/2159256X.2016.1165785
698 1165785 [pii]
699 Horie, M., Honda, T., Suzuki, Y., Kobayashi, Y., Daito, T., Oshida, T., . . . Tomonaga, K.
700 (2010). Endogenous non-retroviral RNA virus elements in mammalian genomes.
701 *Nature, 463*(7277), 84-87. doi: 10.1038/nature08695
702 nature08695 [pii]
703 Katzourakis, A., & Gifford, R. J. (2010). Endogenous viral elements in animal genomes.
704 *PLoS Genet, 6*(11), e1001191. doi: 10.1371/journal.pgen.1001191
705 Kimura, M. (1980). A simple method for estimating evolutionary rates of base
706 substitutions through comparative studies of nucleotide sequences. *J Mol Evol,*
707 *16*(2), 111-120.
708 Kraemer, M. U., Sinka, M. E., Duda, K. A., Mylne, A. Q., Shearer, F. M., Barker, C. M., . .
709 . Hay, S. I. (2015). The global distribution of the arbovirus vectors Aedes aegypti
710 and Ae. albopictus. *Elife, 4*, e08347. doi: 10.7554/eLife.08347
711 Kramer, L. D. (2016). Complexity of virus-vector interactions. *Curr Opin Virol, 21*, 81-86.
712 doi: S1879-6257(16)30104-3 [pii]
713 10.1016/j.coviro.2016.08.008
714 Kramer, L. D., & Ciota, A. T. (2015). Dissecting vectorial capacity for mosquito-borne
715 viruses. *Curr Opin Virol, 15*, 112-118. doi: 10.1016/j.coviro.2015.10.003
716 S1879-6257(15)00153-4 [pii]
717 Lan, Q., & Fallon, A. M. (1990). Small heat shock proteins distinguish between two
718 mosquito species and confirm identity of their cell lines. *Am J Trop Med Hyg,*
719 *43*(6), 669-676.
720 Langmead, B., Trapnell, C., Pop, M., & Salzberg, S. L. (2009). Ultrafast and memory-
721 efficient alignment of short DNA sequences to the human genome. *Genome Biol,*
722 *10*(3), R25. doi: 10.1186/gb-2009-10-3-r25
723 gb-2009-10-3-r25 [pii]
724 Lee, A., Nolan, A., Watson, J., & Tristem, M. (2013). Identification of an ancient
725 endogenous retrovirus, predating the divergence of the placental mammals.
726 *Philos Trans R Soc Lond B Biol Sci, 368*(1626), 20120503. doi:
727 10.1098/rstb.2012.0503
728 rstb.2012.0503 [pii]
729 Lesbats, P., Engelman, A. N., & Cherepanov, P. (2016). Retroviral DNA Integration.
730 *Chem Rev, 116*(20), 12730-12757. doi: 10.1021/acs.chemrev.6b00125
731 Li, C. X., Shi, M., Tian, J. H., Lin, X. D., Kang, Y. J., Chen, L. J., . . . Zhang, Y. Z. (2015).
732 Unprecedented genomic diversity of RNA viruses in arthropods reveals the
733 ancestry of negative-sense RNA viruses. *Elife, 4*. doi: 10.7554/eLife.05378
734 Maringer, K., Yousuf, A., Heesom, K. J., Fan, J., Lee, D., Fernandez-Sesma, A., . . .
735 Davidson, A. D. (2017). Proteomics informed by transcriptomics for
736 characterising active transposable elements and genome annotation in Aedes
737 aegypti. *BMC Genomics, 18*(1), 101. doi: 10.1186/s12864-016-3432-5
738 10.1186/s12864-016-3432-5 [pii]
739 Miesen, P., Girardi, E., & van Rij, R. P. (2015). Distinct sets of PIWI proteins produce
740 arbovirus and transposon-derived piRNAs in Aedes aegypti mosquito cells.
741 *Nucleic Acids Res, 43*(13), 6545-6556. doi: 10.1093/nar/gkv590
742 gkv590 [pii]
743 Miesen, P., Ivens, A., Buck, A. H., & van Rij, R. P. (2016). Small RNA Profiling in
744 Dengue Virus 2-Infected Aedes Mosquito Cells Reveals Viral piRNAs and Novel

745 Host miRNAs. *PLoS Negl Trop Dis, 10*(2), e0004452. doi:
746 10.1371/journal.pntd.0004452
747 PNTD-D-15-01748 [pii]
748 Miesen, P., Joosten, J., & van Rij, R. P. (2016). PIWIs Go Viral: Arbovirus-Derived
749 piRNAs in Vector Mosquitoes. *PLoS Pathog, 12*(12), e1006017. doi:
750 10.1371/journal.ppat.1006017
751 PPATHOGENS-D-16-02114 [pii]
752 Mongelli, V., & Saleh, M. C. (2016). Bugs Are Not to Be Silenced: Small RNA Pathways
753 and Antiviral Responses in Insects. *Annu Rev Virol, 3*(1), 573-589. doi:
754 10.1146/annurev-virology-110615-042447
755 Nene, V., Wortman, J. R., Lawson, D., Haas, B., Kodira, C., Tu, Z. J., . . . Severson, D.
756 W. (2007). Genome sequence of Aedes aegypti, a major arbovirus vector.
757 *Science, 316*(5832), 1718-1723. doi: 1138878 [pii]
758 10.1126/science.1138878
759 Palatini, U., Miesen, P., Carballar-Lejarazu, R., Ometto, L., Rizzo, E., Tu, Z., . . .
760 Bonizzoni, M. (2017). Comparative genomics shows that viral integrations are
761 abundant and express piRNAs in the arboviral vectors Aedes aegypti and Aedes
762 albopictus. *BMC Genomics, 18*(1), 512. doi: 10.1186/s12864-017-3903-3
763 10.1186/s12864-017-3903-3 [pii]
764 Parrish, N. F., Fujino, K., Shiromoto, Y., Iwasaki, Y. W., Ha, H., Xing, J., . . . Tomonaga,
765 K. (2015). piRNAs derived from ancient viral processed pseudogenes as
766 transgenerational sequence-specific immune memory in mammals. *RNA, 21*(10),
767 1691-1703. doi: 10.1261/rna.052092.115
768 rna.052092.115 [pii]
769 Peleg, J. (1968). Growth of arboviruses in monolayers from subcultured mosquito
770 embryo cells. *Virology, 35*(4), 617-619.
771 Price, M. N., Dehal, P. S., & Arkin, A. P. (2009). FastTree: computing large minimum
772 evolution trees with profiles instead of a distance matrix. *Mol Biol Evol, 26*(7),
773 1641-1650. doi: 10.1093/molbev/msp077
774 msp077 [pii]
775 Rosenkranz, D., Rudloff, S., Bastuck, K., Ketting, R. F., & Zischler, H. (2015). Tupaia
776 small RNAs provide insights into function and evolution of RNAi-based
777 transposon defense in mammals. *RNA, 21*(5), 911-922. doi:
778 10.1261/rna.048603.114
779 rna.048603.114 [pii]
780 Rosenkranz, D., & Zischler, H. (2012). proTRAC--a software for probabilistic piRNA
781 cluster detection, visualization and analysis. *BMC Bioinformatics, 13*, 5. doi:
782 10.1186/1471-2105-13-5
783 1471-2105-13-5 [pii]
784 Staginnus, C., Gregor, W., Mette, M. F., Teo, C. H., Borroto-Fernandez, E. G., Machado,
785 M. L., . . . Schwarzacher, T. (2007). Endogenous pararetroviral sequences in
786 tomato (Solanum lycopersicum) and related species. *BMC Plant Biol, 7*, 24. doi:
787 1471-2229-7-24 [pii]
788 10.1186/1471-2229-7-24
789 Sullivan, M. J., Petty, N. K., & Beatson, S. A. (2011). Easyfig: a genome comparison
790 visualizer. *Bioinformatics, 27*(7), 1009-1010. doi: 10.1093/bioinformatics/btr039
791 btr039 [pii]
792 Suzuki, Y., Frangeul, L., Dickson, L. B., Blanc, H., Verdier, Y., Vinh, J., . . . Saleh, M. C.
793 (2017). Uncovering the repertoire of endogenous flaviviral elements in Aedes
794 mosquito genomes. *J Virol*. doi: JVI.00571-17 [pii]
795 10.1128/JVI.00571-17

796 Taylor, D. J., Leach, R. W., & Bruenn, J. (2010). Filoviruses are ancient and integrated
797 into mammalian genomes. *BMC Evol Biol, 10*, 193. doi: 10.1186/1471-2148-10-
798 193
799 1471-2148-10-193 [pii]
800 Thompson, P. J., Macfarlan, T. S., & Lorincz, M. C. (2016). Long Terminal Repeats:
801 From Parasitic Elements to Building Blocks of the Transcriptional Regulatory
802 Repertoire. *Mol Cell, 62*(5), 766-776. doi: 10.1016/j.molcel.2016.03.029
803 S1097-2765(16)30012-0 [pii]
804 Varjak, M., Maringer, K., Watson, M., Sreenu, V. B., Fredericks, A. C., Pondeville, E., . . .
805 Schnettler, E. (2017). Aedes aegypti Piwi4 Is a Noncanonical PIWI Protein
806 Involved in Antiviral Responses. *mSphere, 2*(3). doi: e00144-17 [pii]
807 10.1128/mSphere.00144-17
808 mSphere00144-17 [pii]
809 Vicoso, B., & Bachtrog, D. (2015). Numerous transitions of sex chromosomes in Diptera.
810 *PLoS Biol, 13*(4), e1002078. doi: 10.1371/journal.pbio.1002078
811 PBIOLOGY-D-14-02861 [pii]
812 Watson, M., Schnettler, E., & Kohl, A. (2013). viRome: an R package for the
813 visualization and analysis of viral small RNA sequence datasets. *Bioinformatics,*
814 *29*(15), 1902-1903. doi: 10.1093/bioinformatics/btt297
815 btt297 [pii]
816 Yamanaka, S., Siomi, M. C., & Siomi, H. (2014). piRNA clusters and open chromatin
817 structure. *Mob DNA, 5*, 22. doi: 10.1186/1759-8753-5-22
818 1759-8753-5-22 [pii]
819
820
821

822 **LEGENDS FOR MAIN FIGURES**
823
824 **Figure 1. Contiguity of the *Aedes aegypti* genome is drastically improved in**
825 **the Aag2 assembly.** (A) Histogram of contig length vs. total amount of sequence
826 contained in each bin. The Aag2 assembly achieved the largest contig sizes (by
827 an order of magnitude) compared to previous *Aedes aegypti*-derived assemblies.
828 This large contig size also resulted in more overall sequence information/number
829 of bases. (B) Boxplots indicating number of contigs aligned between LVP
830 (Sanger) and Aag2 (PacBio). When aligned to each other, more contigs from
831 LVP are aligned to larger Aag2 contigs than vice versa.
832
833 **Figure 2. Identification of Endogenous Viral Elements (EVEs) in the Aag2**
834 **assembly** (A) Bar plots showing the number (top) and total length (bottom) of
835 EVEs derived from each viral family. (B) Histogram showing the size distribution
836 of EVEs in the Aag2 genome (top) and the total number of bases pairs derived
837 from EVEs of a given size. The median EVE size (620bp) is indicated with a
838 black bar.
839 (C) Coverage plots of EVEs derived from the viral families (i) Flaviviridae, (ii)
840 Rhabdoviridae, and (iii) Chuviridae. Each bar represents a single EVE, while its
841 length and position denotes the region of the indicated ORF from which its
842 sequence is derived. Length is expressed as a percentage of the total ORF to
843 normalize for varying ORF lengths among different members of a given viral
844 family. The genome organization of CFAV is presented for reference in (i). In (ii)
845 and (iii), a generic genome is presented to illustrate from where EVEs are
846 derived within the genome and within each specific ORF.
847 (D) Phylogenetic relationship between 61 members of Flaviviridae. EVEs present
848 in (i) *Ae. aegytpi* or (ii) *Ae. albopictus* which align to the indicated virus are
849 marked with a colored circle. Size corresponds to abundance of EVEs derived
850 from given species.
851
852 **Figure 3. The repeat landscape of the *Aedes aegypti* genome is**
853 **predominantly made up of transposable elements.** (A) Pie chart representing
854 relative numbers repetitive elements in the Aag2 genome. Further detail can be
855 found in Table 2.
856 (B) Stacked histogram of Kimura divergence for classes of TEs found in the Aag2
857 assembly, expressed as a function of percentage of the genome. A relatively
858 recent expansion/active phase of LTRs is evident (increase in LTRs at low
859 Kimura divergence scores). Kimura divergence scores are based on the
860 accumulated mutations of a given TE sequence compared to a consensus.
861 (C) Histograms showing counts of non-overlapping TEs closest to EVEs binned
862 by distance, both upstream (negative x-axis values) and downstream (positive x-
863 axis values). Positive y-axis counts refer to TE/EVE 'pairs' with the same
864 strandedness , while negative y-axis counts are EVEs where the closest TE has
865 the opposite strandedness. Total counts represented in each histogram: All
866 classes (n=942); LTR only (n=614); No LTRs (n=328); Ty3/gypsy only (n=358);
867 Pao Bel only (n=226); Ty1/copia only (n=30).

868 (D) Heatmap showing categories of TEs nearest EVEs, categorized by the viral
869 family from which the EVEs were derived. Only TEs with the same strandedness
870 as its nearest EVE are shown. A "*" indicates significant enrichment by one-sided
871 binomial test against the background prevalence of a given TE category in the
872 genome (eg among all LTRs nearest Chuviridae-derived EVEs, Pao Bel
873 elements are specifically enriched compared to the genome-wide counts of Pao
874 Bel among all LTRs). Color indicates proportion of a given TE category nearest
875 EVEs derived from the indicated viral family. Grey indicates the element was not
876 found to be the closest TE to any EVEs derived from the indicated viral family.
877 Only TE elements which made up at least 10% of the dataset for a given viral
878 family are shown. "Pao Bel elements" refers to Chuviridae, while "Ty3/gypsy
879 elements" corresponds to Flaviviridae and Rhabdoviridae. Total sample size of
880 all TEs analyzed for each dataset: LTRs- Rhabdoviridae (n=130),Flaviviridae
881 (n=181), Chuviridae (n=107); Pao Bel- Chuviridae (n=84); Ty3/gypsy-
882 Rhabdoviridae (n=100), Flaviviridae (n=136).
883
884 **Figure 4. EVEs are primarily associated with LTR transposable elements.**
885 (A) Circle plot showing the arrangement and diversity of TE subclasses in the ten
886 largest contigs in the Aag2 assembly. Individual contigs are denoted with
887 staggered black bars. Specific TE elements are shown as dots, concentric rngs
888 represent individual families within each TE subclass. Large scale fluctuations in
889 TE density can be seen in specific contigs (contig 000015F, boxed).
890 (B) Local density plots of a representative region of local LTR density in contig
891 000015F.
892 (C) The regions of local LTR density corresponds to the location of numerous
893 EVEs (black arrows) and piRNA density (bar chart, bottom track).
894 Bioinformatically predicted piCluster corresponding to a portion of the large LTR
895 density in contig 000015F. LTRs (shown as black bars) are interspersed with
896 EVE sequences (colored by virus family). piRNA production (black bars, below)
897 shows highest density in regions corresponding to EVE sequences.
898 (D) Dotplot showing the relationship between piCluster EVE content and piRNA
899 production. piClusters are ranked by piRNA production. (E) Violin plot comparing
900 the distribution of piRNA density in piClusters with or without EVEs. (F) Violin
901 plots comparing the number of predicted transcription factor binding sites in
902 piClusters with or without EVEs.
903
904 **Figure 5. The antiviral potential of the cellular piRNA repertoire.**
905 (A) Bar plot showing the proportion of piRNA mapping to EVE sequences from a
906 given viral family. Bars are split to show the relative contribution of specific EVE
907 sequences.
908 (B) Plot showing correlation the genomic footprint of EVEs from specific viral
909 families in the Aag2 genome and their piRNA production. Bunyavirus and
910 Chuvirus fall on opposite sides of the trend.
911 (C) The EVE responsible for producing the anti-sense piRNA in (D). A spike of
912 piRNAs is produced from the EVE (highlighted in orange) within the overall
913 piCluster.

914 (D) Mapping of cellular piRNAs to the bunyavirus PCLV genome reveals the
915 pattern of piRNA processing. The sense-piRNA peak is offset by 10-bp from the
916 antisense-piRNA peak (which also maps to an EVE within the Aag2 genome;
917 blue line), showing a distinct ping-pong like pattern (highlighted by the grey
918 rectangle. Interestingly, although the sequence of the antisense piRNAs map
919 perfectly to the Aag2 genome/EVE, the sense piRNAs map perfectly to the PCLV
920 virus sequence. piRNA counts are determined by the position of each piRNAs 5'
921 base. (E) Schematic showing the process of ping-pong piRNA amplification in
922 the cell. An EVE sequence in a piCluster is transcribed to yield an antigenomic
923 transcript. This transcript is processed into piRNAs which bind the genome of
924 infecting viruses. Binding triggers processing of the viral genome into genomic
925 piRNAs, which bind anti-genomic transcripts, leading to increased processing.
926
927

LEGENDS FOR SUPPLEMENTARY FIGURES

S1 Fig. Transposons are distributed throughout the entire Aag2 genome. (A) Similar plot to Figure 2A, but showing all contigs of the Aag2 assembly. Circular plot of the Aag2 assembly, with every contig (black rectangles; ordered by size) and transposable element (circles; colored by TE class). Transposable elements are prevalent throughout the entire *Ae. aegypti* genome. Rectangles representing contigs are staggered to indicate relative contig size.

S2 Fig. TEs which overlap EVEs are also overrepresented by LTR elements. (A) Histograms of TEs which overlap EVEs, broken down by the following categories. The left bin represents TEs whose start is upstream, and end overlaps the EVE. The 4th bin indicates TEs whose end is downstream, and start overlaps an EVE. The second bin indicates EVEs whose coordinates surround the TE.The third bin indicates TEs whose coordinates surround an EVE. Positive count values indicate TE and EVEs with shared directionality, while negative values represent TE and EVEs with opposite directionality. Some EVEs showed multiple overlapping TEs, all of which are represented on the charts.

S3 Fig. EVEs are typically found within unidirectional piRNA clusters. The left panels correspond to a region of Contig 000933F encoding 4 tandem, unidirectional piRNA clusters (as identified by proTRAC), each containing EVEs. Each cluster expresses piRNAs primarily anti-sense to the TEs/EVEs which define them. Similarly, a single large piRNA cluster on Contig 000044F is shown in the right panels. The shared directionality between TEs and EVEs (Figure 3B) is evident. Again, piRNA expression is almost exclusively in the antisense direction with respect to the TEs/EVEs.

S4 Fig. Kimura divergence scores of LTRs only show expansion of Pao Bel and Ty3/gypsy elements. Bar plot of kimura scores assigned to LTRs only, categorized by TE family and expressed as percent of total genome (as in Figure 2E). At very low (0-1) Kimura divergence scores, Ty3/gypsy and Pao Bel exhibit a marked increase in proportion of the genome.

S5 Fig. piRNA mapping to various viruses. (A) Same plot as Fig 5D, but showing the entire PCLV nucleocapsid region. (B) piRNAs mapping to Kamiti River Virus do not show the distinct ping-pong signature as seen for PCLV, despite a significant antisense piRNA peak deriving from an EVE.

Figure 1

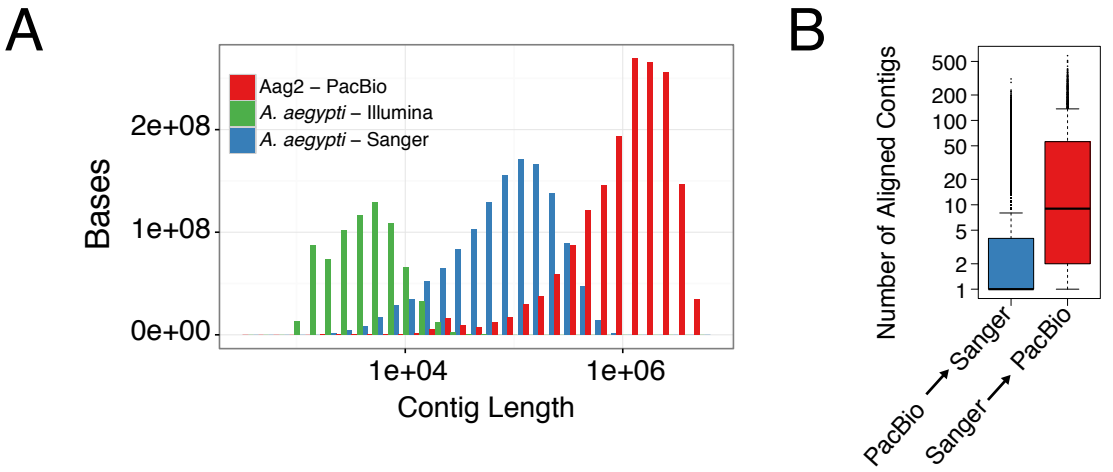
A
Aag2 – PacBio
A. aegypti – Illumina
A. aegypti – Sanger
Bases
2e+08
1e+08
0e+00
1e+04
1e+06
Contig Length
B
Number of Aligned Contigs
500
200
100
50
20
10
5
2
1
PacBio → Sanger
Sanger → PacBio

Figure 2

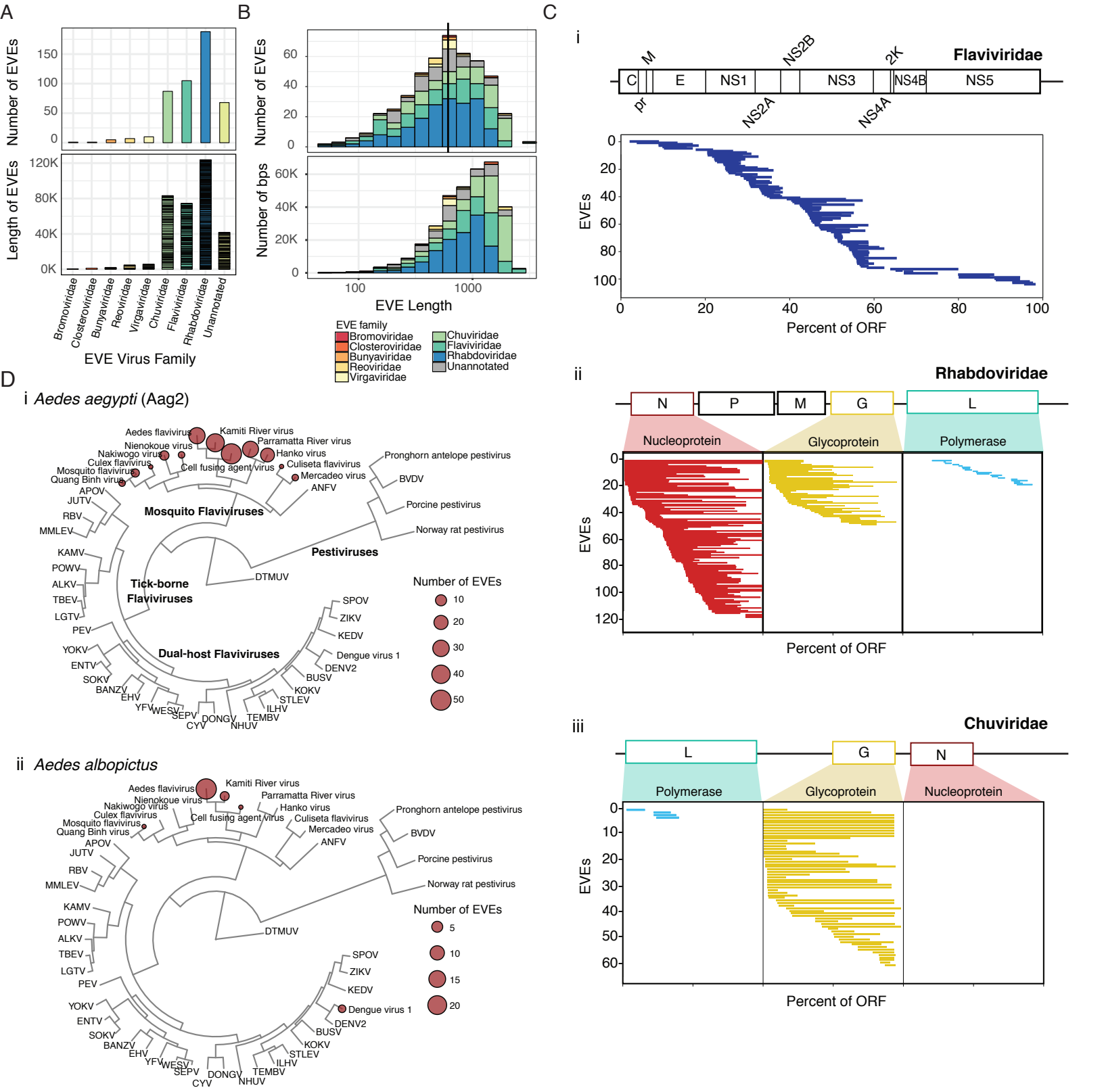
A
Number of EVEs
Length of EVEs
Bromoviridae
Closteroviridae
Bunyaviridae
Reoviridae
Virgaviridae
Chuviridae
Flaviviridae
Rhabdoviridae
Unannotated
EVE Virus Family
B
Number of EVEs
Number of bps
EVE Length
EVE family
Bromoviridae
Closteroviridae
Bunyaviridae
Reoviridae
Virgaviridae
Chuviridae
Flaviviridae
Rhabdoviridae
Unannotated
C
i
Flaviviridae
M
NS2B
2K
C
E
NS1
NS3
NS4B
NS5
pr
NS2A
NS4A
EVEs
Percent of ORF
ii
Rhabdoviridae
N
P
M
G
L
Nucleoprotein
Glycoprotein
Polymerase
EVEs
Percent of ORF
iii
Chuviridae
L
G
N
Polymerase
Glycoprotein
Nucleoprotein
EVEs
Percent of ORF
D
i Aedes aegypti (Aag2)
Aedes flavivirus
Kamiti River virus
Nienokoue virus
Parramatta River virus
Nakiwogo virus
Hanko virus
Culex flavivirus
Cell fusing agent virus
Culiseta flavivirus
Mosquito flavivirus
Mercadeo virus
Quang Binh virus
ANFV
APOV
JUTV
RBV
MMLEV
Mosquito Flaviviruses
Pronghorn antelope pestivirus
BVDV
Porcine pestivirus
Norway rat pestivirus
Pestiviruses
KAMV
POWV
ALKV
TBEV
LGTV
PEV
DTMUV
Tick-borne Flaviviruses
SPOV
ZIKV
KEDV
Dengue virus 1
DENV2
BUSV
KOKV
STLEV
ILHV
TEMBV
NHUV
DONGV
CYV
SEPV
WESV
YFV
EHV
BANZV
SOKV
ENTV
YOKV
Dual-host Flaviviruses
Number of EVEs
10
20
30
40
50
ii Aedes albopictus
Aedes flavivirus
Kamiti River virus
Nienokoue virus
Parramatta River virus
Nakiwogo virus
Hanko virus
Culex flavivirus
Cell fusing agent virus
Culiseta flavivirus
Mosquito flavivirus
Mercadeo virus
Quang Binh virus
ANFV
APOV
JUTV
RBV
MMLEV
Pronghorn antelope pestivirus
BVDV
Porcine pestivirus
Norway rat pestivirus
KAMV
POWV
ALKV
TBEV
LGTV
PEV
DTMUV
Number of EVEs
5
10
15
20
SPOV
ZIKV
KEDV
Dengue virus 1
DENV2
BUSV
KOKV
STLEV
ILHV
TEMBV
NHUV
DONGV
CYV
SEPV
WESV
YFV
EHV
BANZV
SOKV
ENTV
YOKV

Figure 3

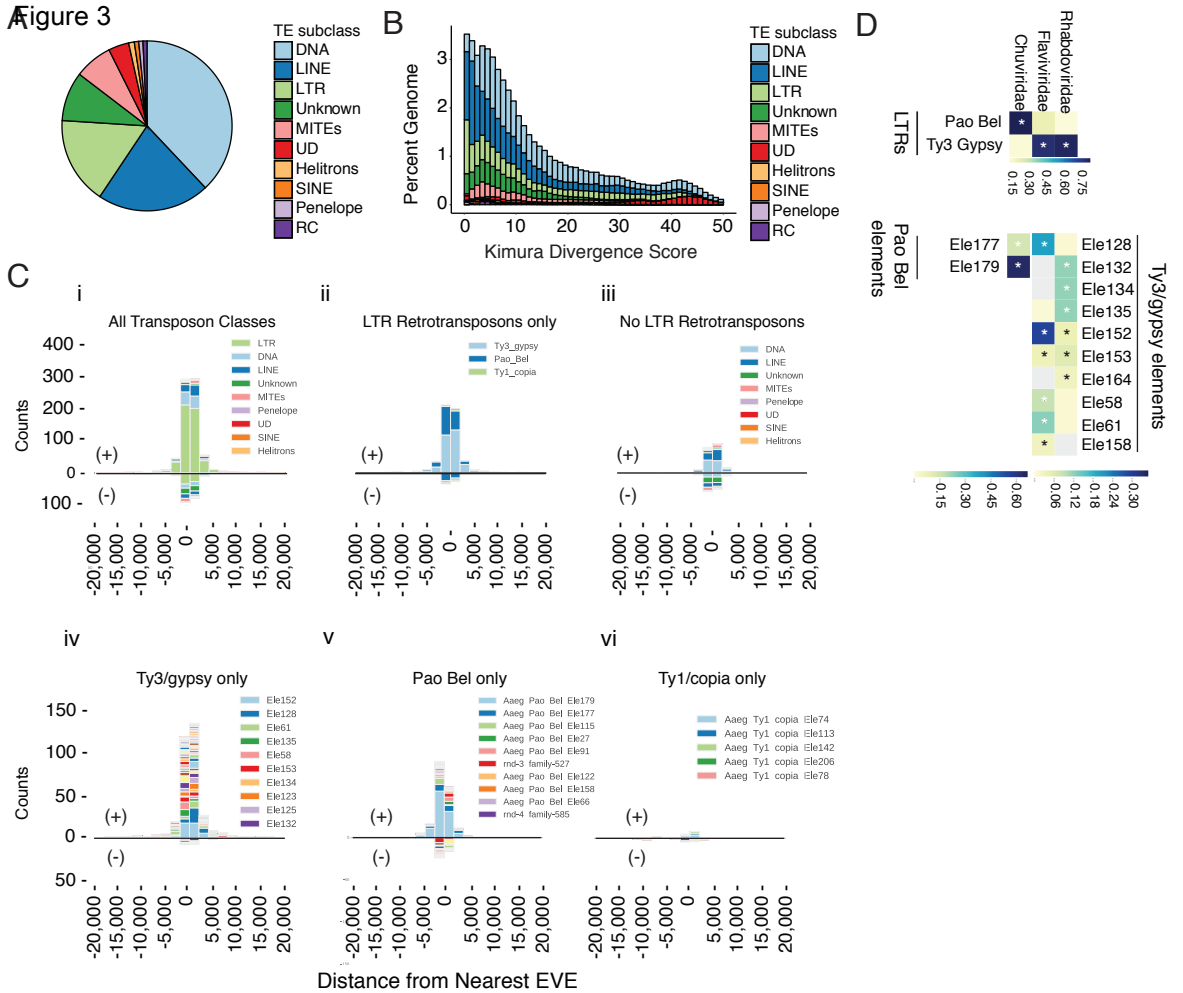
A
TE subclass
DNA
LINE
LTR
Unknown
MITEs
UD
Helitrons
SINE
Penelope
RC
B
Percent Genome
Kimura Divergence Score
C
i
All Transposon Classes
ii
LTR Retrotransposons only
iii
No LTR Retrotransposons
iv
Ty3/gypsy only
v
Pao Bel only
vi
Ty1/copia only
Counts
(+)
(-)
Distance from Nearest EVE
D
Chuviridae
Flaviviridae
Rhabdoviridae
LTRs
Pao Bel
Ty3 Gypsy
Pao Bel elements
Ele177
Ele179
Ty3/gypsy elements
Ele128
Ele132
Ele134
Ele135
Ele152
Ele153
Ele164
Ele58
Ele61
Ele158

Figure 4

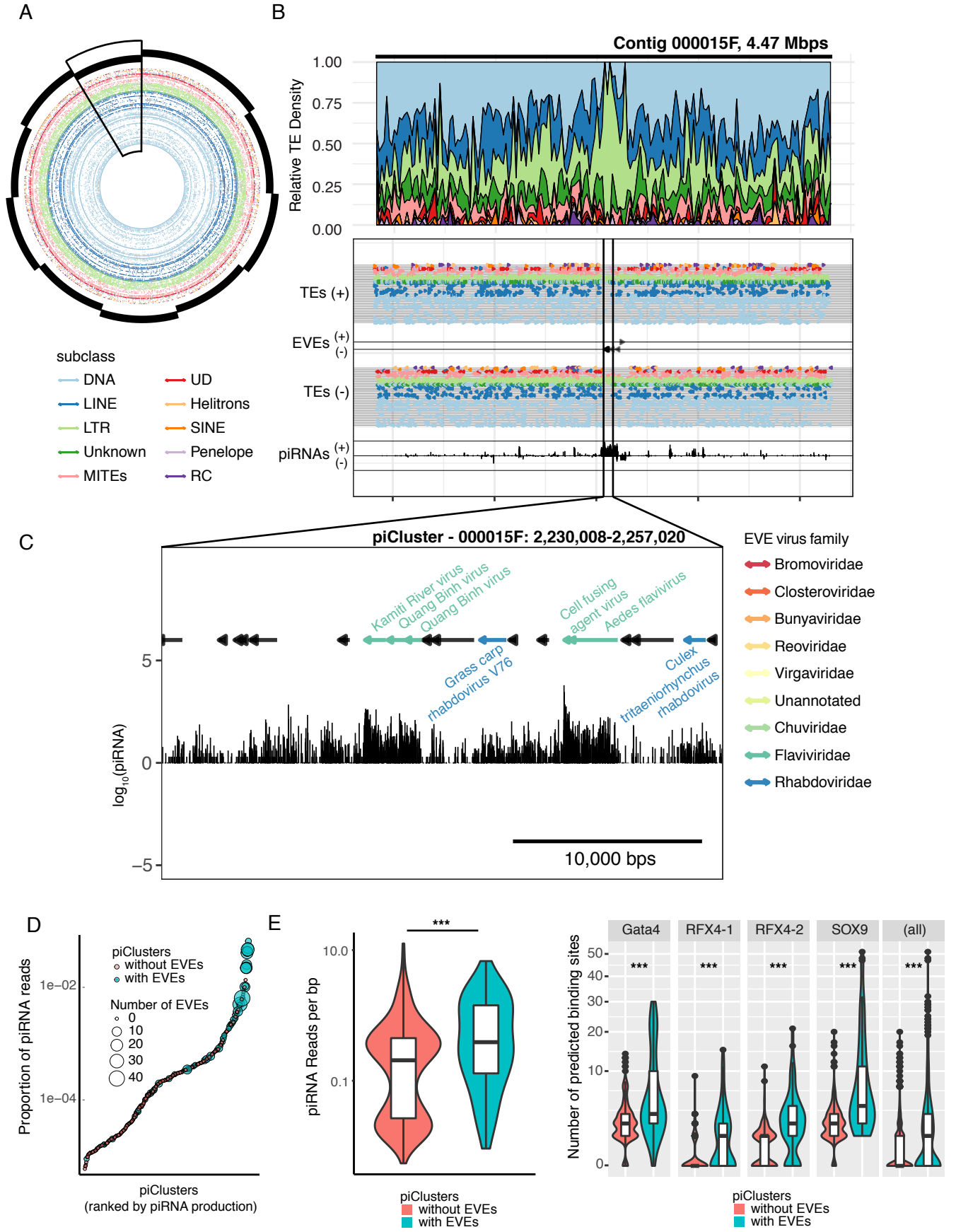
A
B
Contig 000015F, 4.47 Mbps
Relative TE Density
1.00
0.75
0.50
0.25
0.00
TEs (+)
EVEs (+) (-)
TEs (-)
piRNAs (+) (-)
subclass
DNA
LINE
LTR
Unknown
MITEs
UD
Helitrons
SINE
Penelope
RC
C
piCluster - 000015F: 2,230,008-2,257,020
Kamiti River virus
Quang Binh virus
Quang Binh virus
Cell fusing agent virus
Aedes flavivirus
Grass carp rhabdovirus V76
Culex tritaeniorhynchus rhabdovirus
log10(piRNA)
5
0
−5
10,000 bps
EVE virus family
Bromoviridae
Closteroviridae
Bunyaviridae
Reoviridae
Virgaviridae
Unannotated
Chuviridae
Flaviviridae
Rhabdoviridae
D
Proportion of piRNA reads
1e−02
1e−04
piClusters
without EVEs
with EVEs
Number of EVEs
0
10
20
30
40
piClusters
(ranked by piRNA production)
E
***
piRNA Reads per bp
10.0
0.1
piClusters
without EVEs
with EVEs
Gata4
RFX4-1
RFX4-2
SOX9
(all)
Number of predicted binding sites
50
40
30
20
10
0
***
piClusters
without EVEs
with EVEs

Figure 5

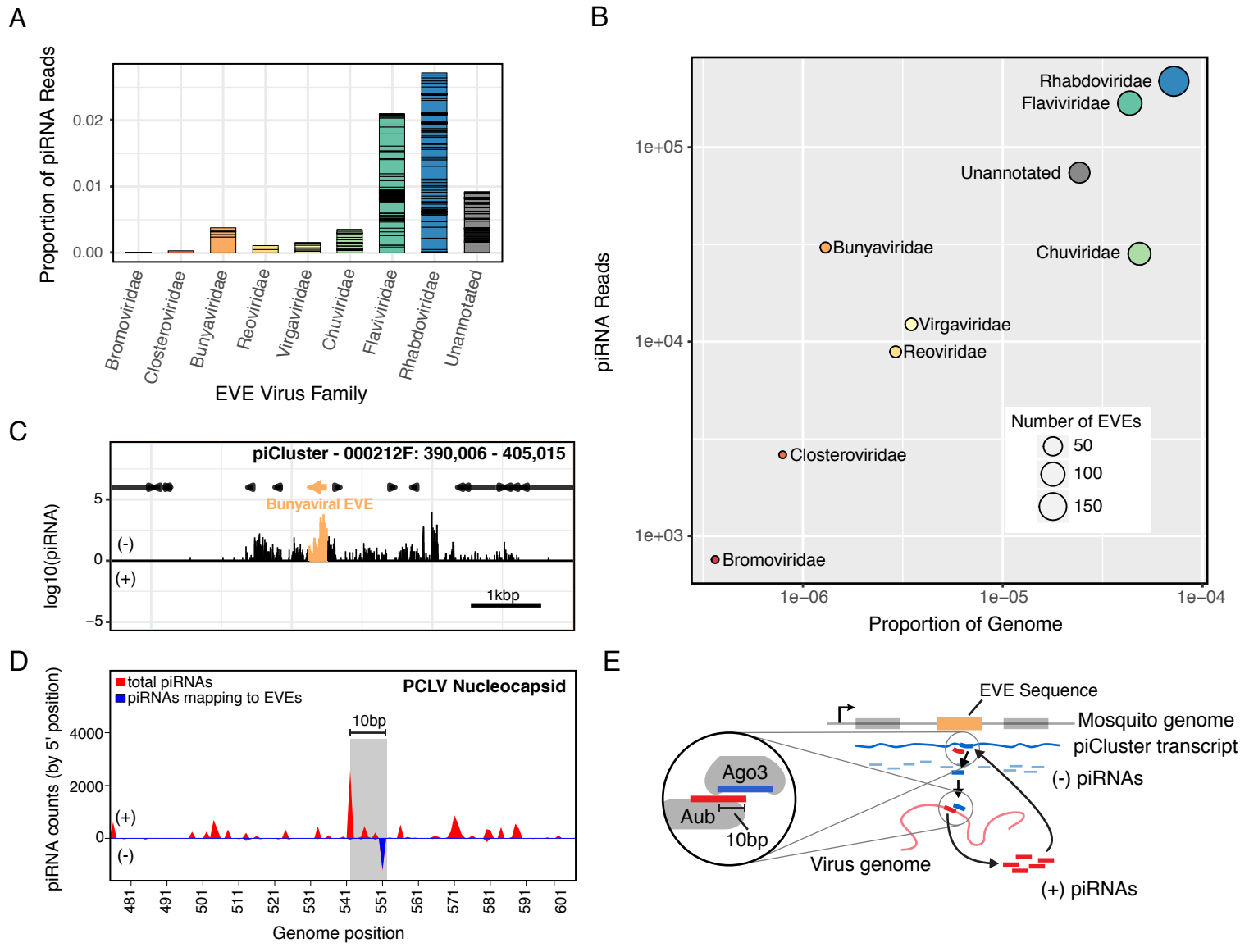
A
Proportion of piRNA Reads
0.02
0.01
0.00
Bromoviridae
Closteroviridae
Bunyaviridae
Reoviridae
Virgaviridae
Chuviridae
Flaviviridae
Rhabdoviridae
Unannotated
EVE Virus Family
B
piRNA Reads
1e+05
1e+04
1e+03
Rhabdoviridae
Flaviviridae
Unannotated
Bunyaviridae
Chuviridae
Virgaviridae
Reoviridae
Closteroviridae
Bromoviridae
Number of EVEs
50
100
150
1e−06
1e−05
1e−04
Proportion of Genome
C
piCluster - 000212F: 390,006 - 405,015
Bunyaviral EVE
log10(piRNA)
5
0
−5
(-)
(+)
1kbp
D
total piRNAs
piRNAs mapping to EVEs
PCLV Nucleocapsid
10bp
piRNA counts (by 5' position)
4000
2000
0
(+)
(-)
481
491
501
511
521
531
541
551
561
571
581
591
601
Genome position
E
EVE Sequence
Mosquito genome
piCluster transcript
(-) piRNAs
Ago3
Aub
10bp
Virus genome
(+) piRNAs

Figure S1

Click here to download Supplemental Data S1Fig_PD.png

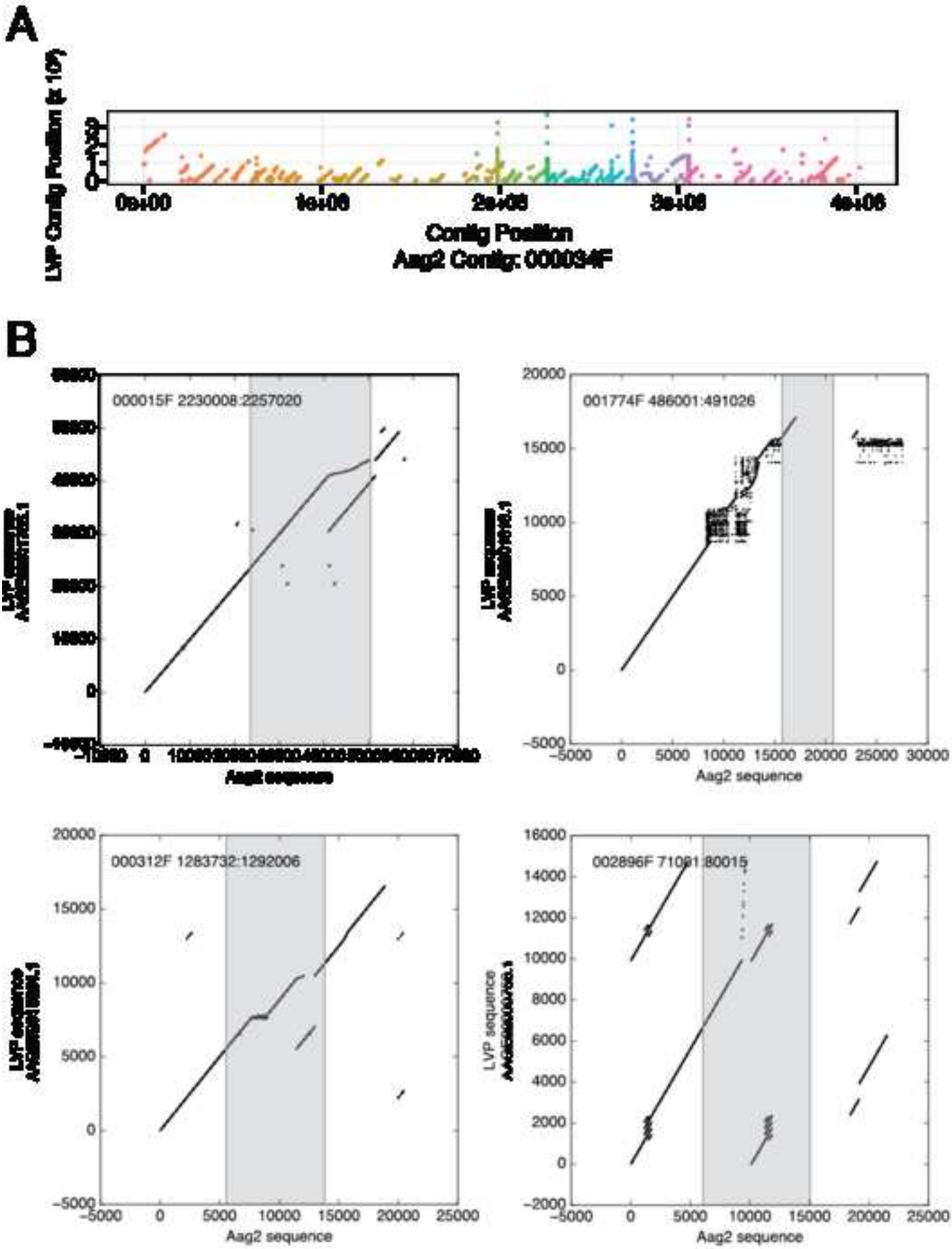

Figure S2

A

Overlapping TE/EVE pairs

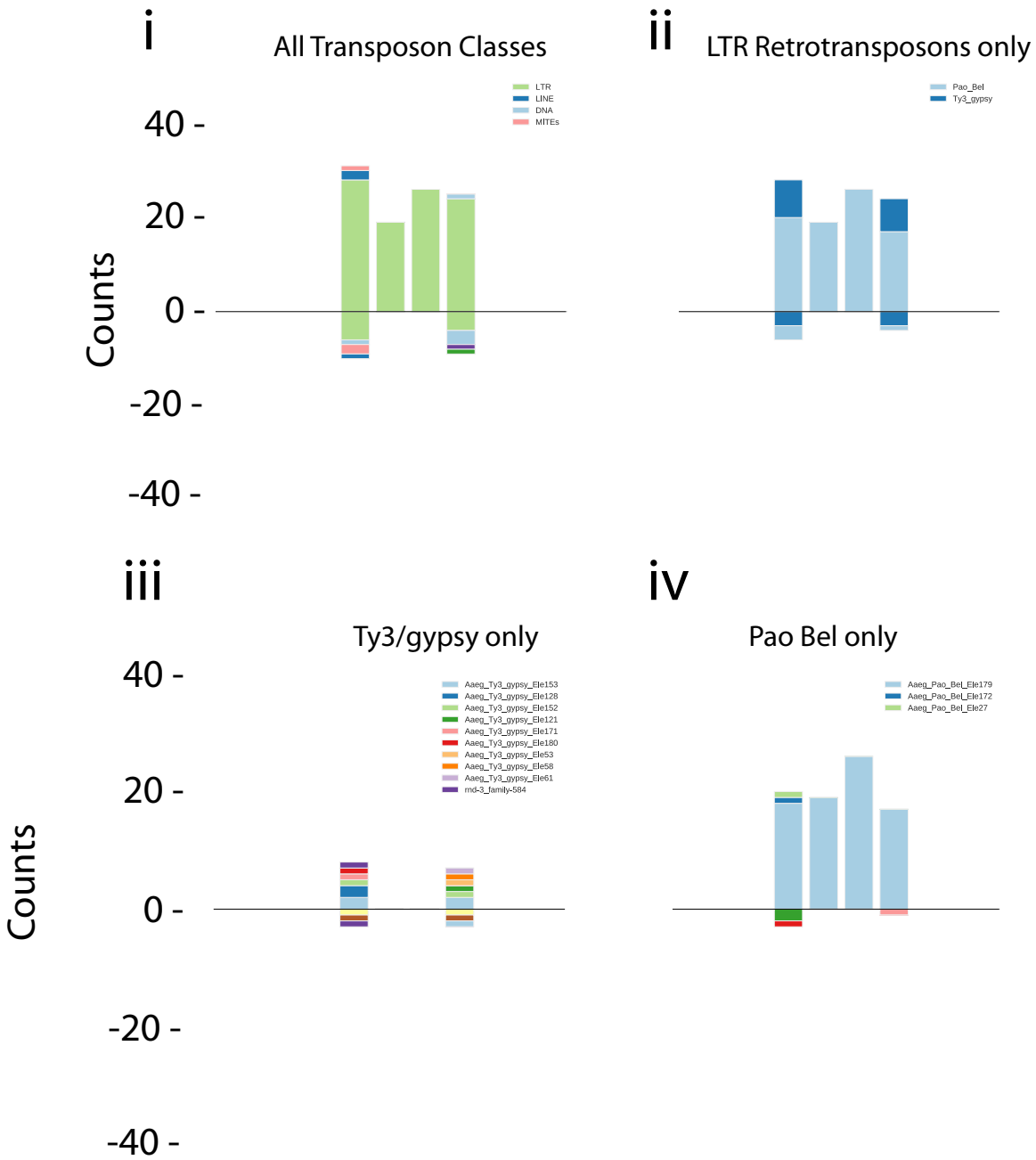

Figure S3

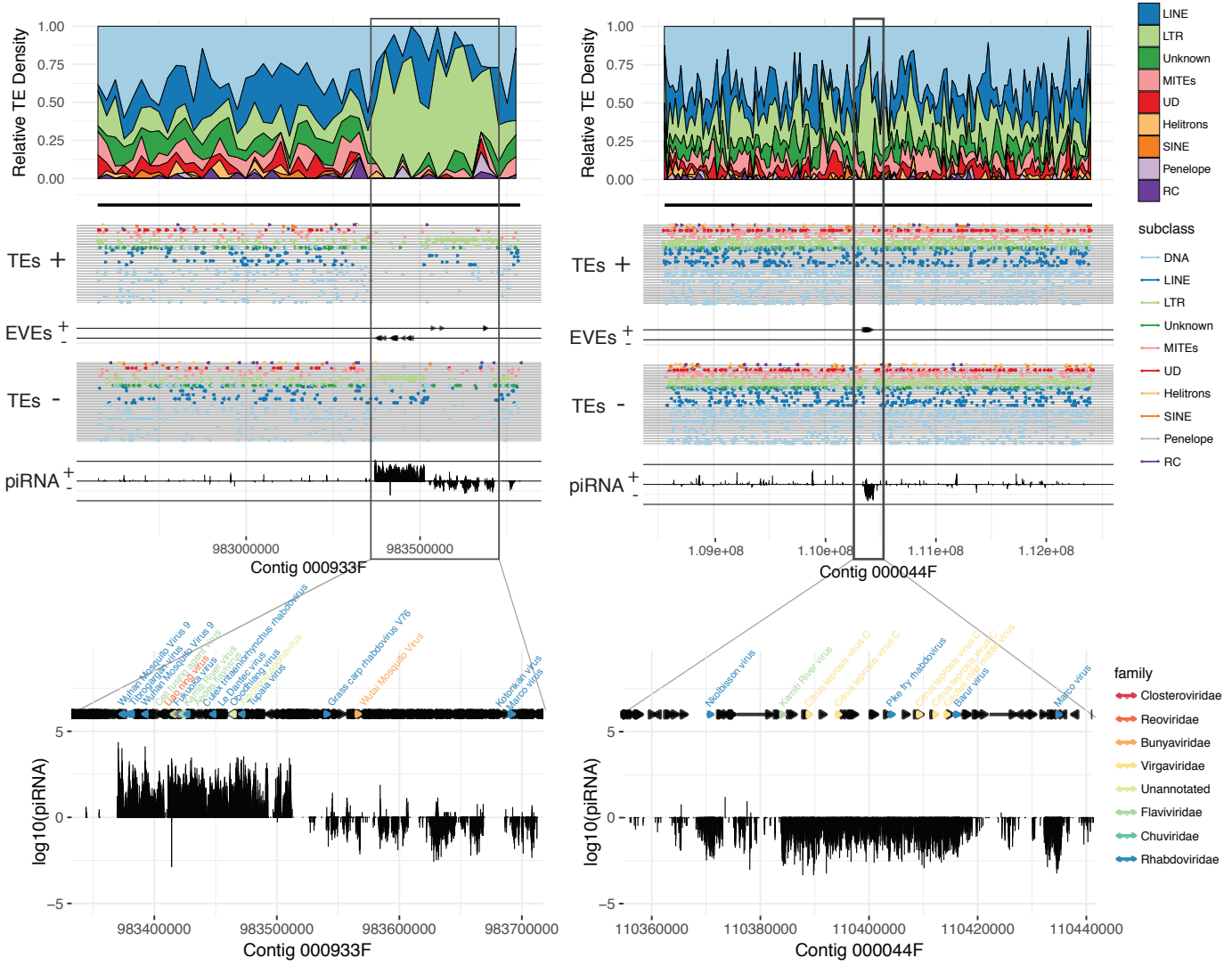

Relative TE Density
1.00
0.75
0.50
0.25
0.00
TEs +
EVEs +
-
TEs -
piRNA +
-
983000000
983500000
Contig 000933F
1.09e+08
1.10e+08
1.11e+08
1.12e+08
Contig 000044F
LINE
LTR
Unknown
MITEs
UD
Helitrons
SINE
Penelope
RC
subclass
DNA
LINE
LTR
Unknown
MITEs
UD
Helitrons
SINE
Penelope
RC
Wuhan Mosquito Virus 9
Tibrogargan virus
Wuhan Mosquito Virus 9
Cutlet Mountain virus
Lake Ning virus
Pikuda virus
Culex Mitrasinorhynchus rhabdovirus
Le Dantec virus
Obodhiang virus
Tupaia virus
Grass carp rhabdovirus V76
Wutai Mosquito Virus
Kotonkan virus
Marco virus
Nkolbisson virus
Kamiti River virus
Citrus leprosis virus C
Citrus leprosis virus C
Pike fry rhabdovirus
Citrus leprosis virus C
Citrus leprosis virus C
Barur virus
Marco virus
family
Closteroviridae
Reoviridae
Bunyaviridae
Virgaviridae
Unannotated
Flaviviridae
Chuviridae
Rhabdoviridae
log10(piRNA)
5
0
−5
983400000
983500000
983600000
983700000
Contig 000933F
110360000
110380000
110400000
110420000
110440000
Contig 000044F

Figure S4

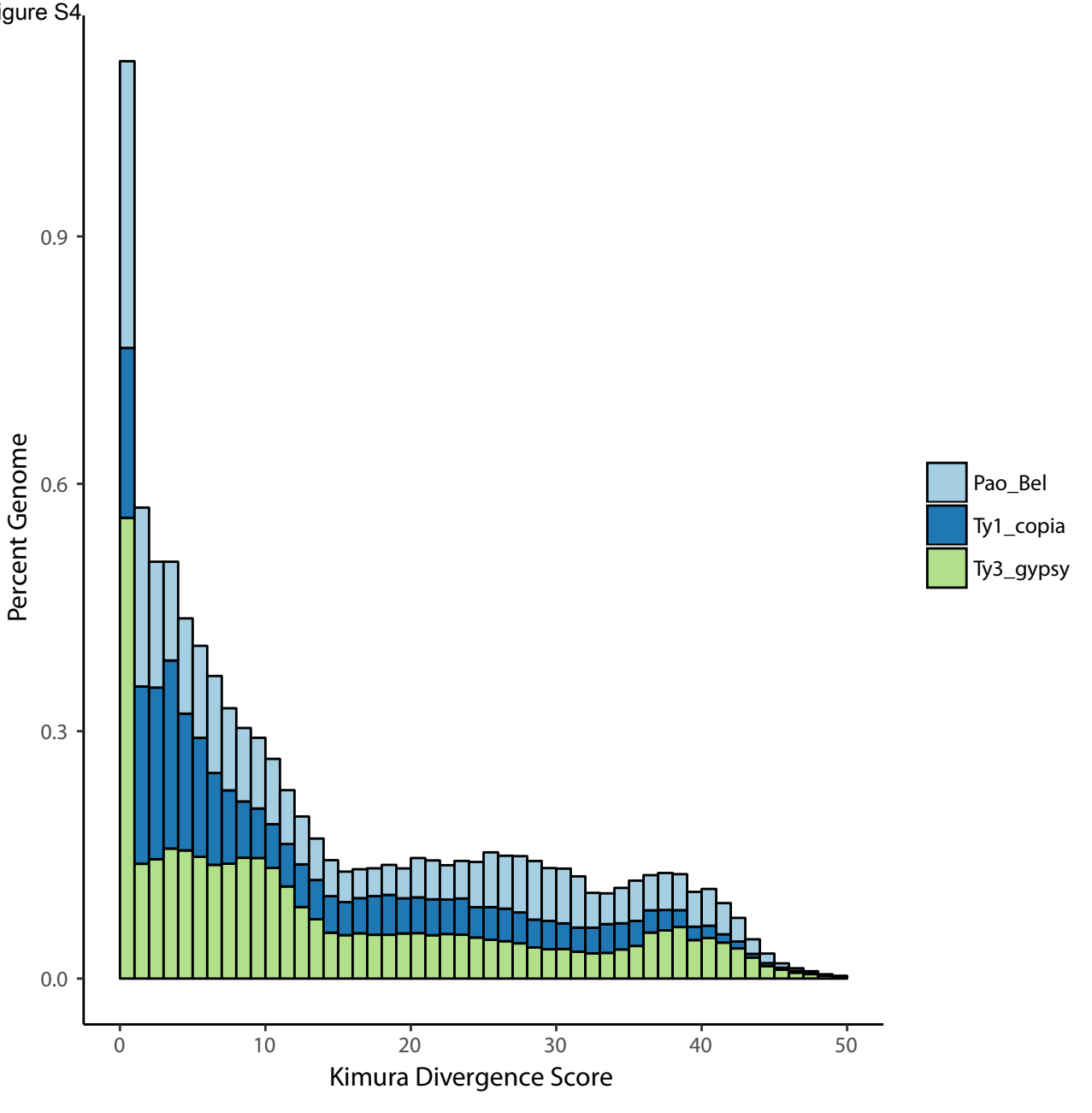
Percent Genome
0.0
0.3
0.6
0.9
0
10
20
30
40
50
Kimura Divergence Score
Pao_Bel
Ty1_copia
Ty3_gypsy

Figure S5

A

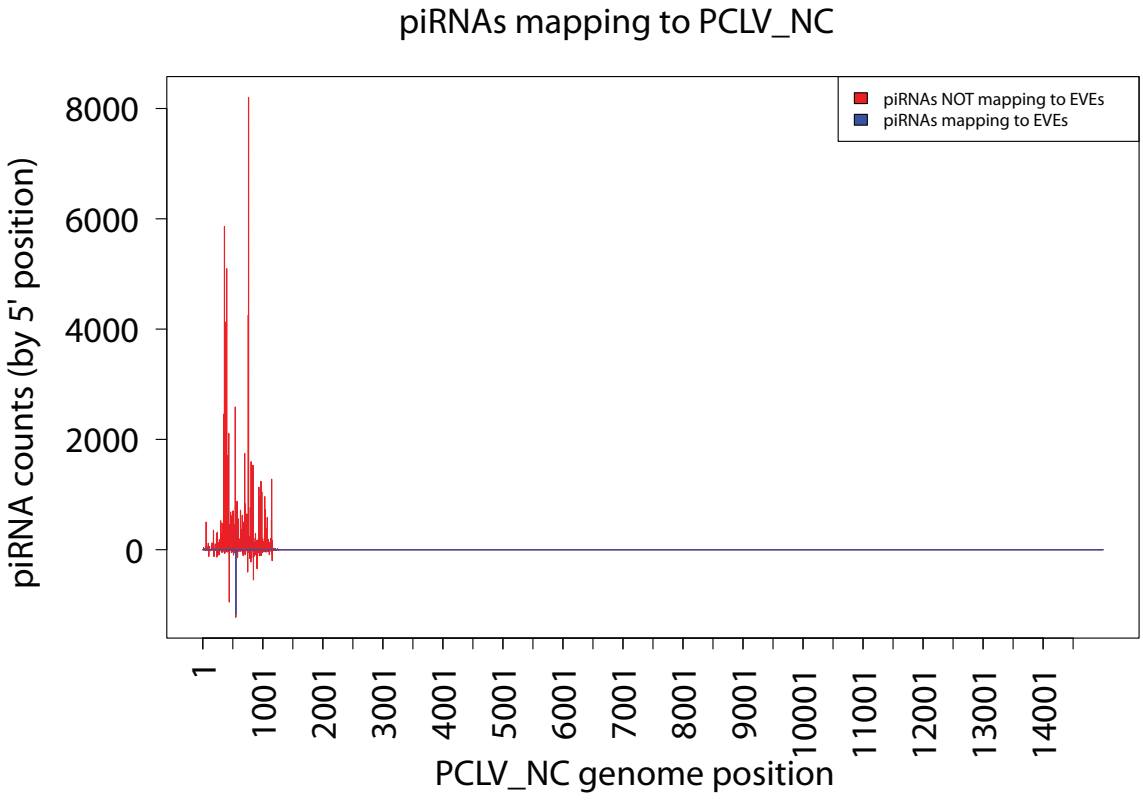
piRNAs mapping to PCLV_NC
piRNAs NOT mapping to EVEs
piRNAs mapping to EVEs
piRNA counts (by 5' position)
8000
6000
4000
2000
0
1
1001
2001
3001
4001
5001
6001
7001
8001
9001
10001
11001
12001
13001
14001
PCLV_NC genome position

B

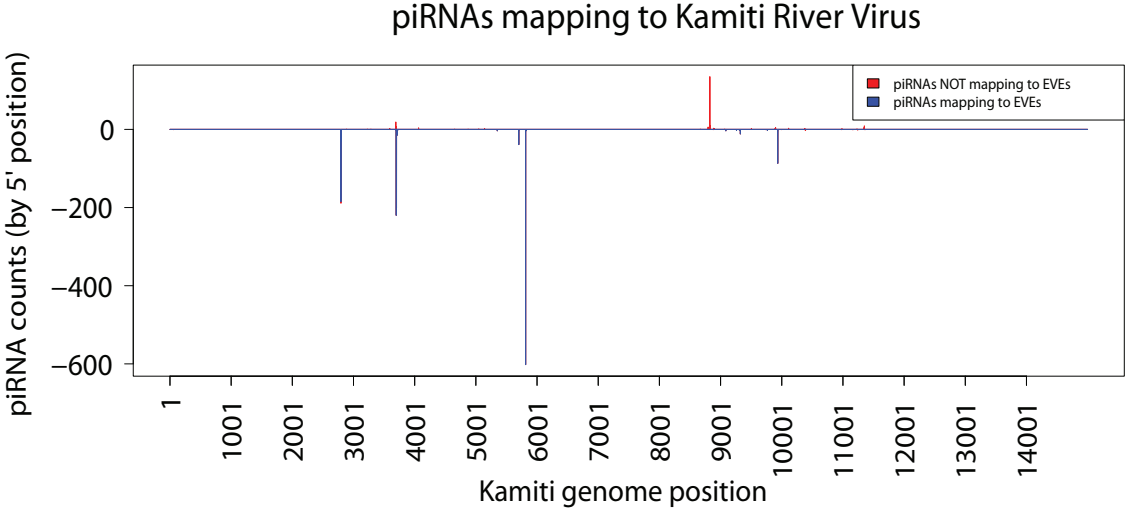
piRNAs mapping to Kamiti River Virus
piRNAs NOT mapping to EVEs
piRNAs mapping to EVEs
piRNA counts (by 5' position)
0
−200
−400
−600
1
1001
2001
3001
4001
5001
6001
7001
8001
9001
10001
11001
12001
13001
14001
Kamiti genome position

Table 1

	UCB	LVP	Aag2
Sample	LVP strain	LVP strain	Aag2 cell line
Seq. Strategy	Illumina	Sanger	PacBio
Released	5/2015	6/2006	NA
Coverage	6.8x	7.6x	~50x
Total sequence length	744,596,036	1,383,957,531	1,723,930,323
Total assembly gap length	196,533,049	73,881,199	0
Num. of contigs	961,292	36,204	3,752
Contig N50	989	82,618	1,420,116
Contig L50	151,087	4,346	368

Table 2

	Num. of elements	Length (Mbp)	Percent of genome
SINE	28,301	4.4	0.25
LINE	558,382	259.9	15.07
LTR	495,204	163.9	9.51
DNA	1,184,522	309.0	17.93
Other*	725,958	233.7	13.55
Total	2,992,367	970.9	56.31

*includes helitrons, MITEs, Penelope, RC, UD, and unknown elements